

This is a repository copy of *Impacts of bromine and iodine chemistry on tropospheric OH and HO₂ : Comparing observations with box and global model perspectives*.

White Rose Research Online URL for this paper:
<https://eprints.whiterose.ac.uk/122677/>

Version: Published Version

Article:

Stone, Daniel, Sherwen, Toms orcid.org/0000-0002-3006-3876, Evans, Mathew J. orcid.org/0000-0003-4775-032X et al. (10 more authors) (2018) Impacts of bromine and iodine chemistry on tropospheric OH and HO₂ : Comparing observations with box and global model perspectives. *Atmospheric Chemistry and Physics*. pp. 3541-3561. ISSN 1680-7324

<https://doi.org/10.5194/acp-18-3541-2018>

Reuse

This article is distributed under the terms of the Creative Commons Attribution (CC BY) licence. This licence allows you to distribute, remix, tweak, and build upon the work, even commercially, as long as you credit the authors for the original work. More information and the full terms of the licence here:
<https://creativecommons.org/licenses/>

Takedown

If you consider content in White Rose Research Online to be in breach of UK law, please notify us by emailing eprints@whiterose.ac.uk including the URL of the record and the reason for the withdrawal request.



1 Impacts of bromine and iodine chemistry on tropospheric OH and HO₂: 2 Comparing observations with box and global model perspectives

3
4 Daniel Stone,¹ Tomás Sherwen,² Mathew J. Evans,^{2,3} Stewart Vaughan,¹ Trevor Ingham,^{1,4}
5 Lisa K. Whalley,^{1,4} Peter M. Edwards,² Katie A. Read,^{2,3} James D. Lee,^{2,3} Sarah J. Moller,^{2,3}
6 Lucy J. Carpenter,^{2,3} Alastair C. Lewis,^{2,3} Dwayne E. Heard^{1,4}

7
8 ¹ School of Chemistry, University of Leeds, Leeds, UK

9 ² Wolfson Atmospheric Chemistry Laboratories, Department of Chemistry, University of York, York, UK

10 ³ National Centre for Atmospheric Science, University of York, York, UK

11 ⁴ National Centre for Atmospheric Science, University of Leeds, Leeds, UK

12 13 14 Abstract

15 The chemistry of the halogen species bromine and iodine has a range of impacts on tropospheric composition,
16 and can affect oxidising capacity in a number of ways. However, recent studies disagree on the overall sign of
17 the impacts of halogens on the oxidising capacity of the troposphere. We present simulations of OH and HO₂
18 radicals for comparison with observations made in the remote tropical ocean boundary layer during the Seasonal
19 Oxidant Study at the Cape Verde Atmospheric Observatory in 2009. We use both a constrained box model, using
20 detailed chemistry derived from the Master Chemical Mechanism (v3.2), and the three-dimensional global
21 chemistry transport model GEOS-Chem. Both model approaches reproduce the diurnal trends in OH and HO₂.
22 Absolute observed concentrations are well reproduced by the box model but are overpredicted by the global
23 model, potentially owing to incomplete consideration of oceanic sourced radical sinks. The two models, however,
24 differ in the impacts of halogen chemistry. In the box model, halogen chemistry acts to increase OH
25 concentrations (by 9.8 % at midday at Cape Verde), while the global model exhibits a small increase in OH at
26 Cape Verde (by 0.6 % at midday) but overall shows a decrease in the global annual mass weighted mean OH of
27 4.5 %. These differences reflect the variety of timescales through which the halogens impact the chemical system.
28 On short timescales, photolysis of HOBr and HOI, produced by reactions of HO₂ with BrO and IO, respectively,
29 increases the OH concentration. On longer timescales, halogen catalysed ozone destruction cycles lead to lower
30 primary production of OH radicals through ozone photolysis, and thus to lower OH concentrations. The global
31 model includes more of the longer timescale responses than the constrained box model and overall the global
32 impact of the longer timescale response (reduced primary production due to lower O₃ concentrations) overwhelms
33 the shorter timescale response (enhanced cycling from HO₂ to OH), and thus the global OH concentration
34 decreases. The Earth system contains many such responses on a large range of timescales. This work highlights
35 the care that needs to be taken to understand the full impact of any one process on the system as a whole.



36 Introduction

37 Halogen chemistry in the troposphere influences budgets of O₃, HO_x (OH and HO₂), NO_x (NO and NO₂) (von
38 Glasow et al., 2004; Saiz-Lopez and von Glasow, 2012; Simpson et al., 2015, Schmidt et al., 2016; Sherwen et
39 al., 2016a; Sherwen et al., 2016b), affects the oxidation state of atmospheric mercury (Holmes et al., 2006; Holmes
40 et al., 2010), and impacts aerosol formation (Hoffmann et al., 2001; O'Dowd et al., 2002; McFiggans et al., 2004;
41 McFiggans et al., 2010; Mahajan et al., 2011; Sherwen et al., 2016c).

42
43 The production of bromine and iodine atoms in the marine boundary layer (MBL) following emissions of
44 organohalogen compounds and the inorganic compounds I₂ and HOI has been shown to result in considerable
45 destruction of tropospheric ozone (Read et al., 2008), leading to the production of bromine monoxide (BrO) and
46 iodine monoxide (IO) radicals. Observations of BrO and IO radicals within the MBL have demonstrated
47 widespread impacts on atmospheric composition and chemistry (Alicke et al., 1999; Sander et al., 2003; Leser et
48 al., 2003; Saiz-Lopez and Plane, 2004; Saiz-Lopez et al., 2004; Peters et al., 2005; Saiz-Lopez et al., 2006;
49 Whalley et al., 2007; Mahajan et al., 2010a; Commane et al., 2011; Dix et al., 2013; Gomez Martin et al., 2013),
50 including significant effects on HO_x concentrations and on the HO₂:OH ratio in coastal and marine locations
51 (Bloss et al., 2005a; Sommariva et al., 2006; Bloss et al., 2007; Bloss et al., 2010; Kanaya et al., 2007; Whalley
52 et al., 2010).

53
54 The role of halogens in in HO_x chemistry was demonstrated during the NAMBLEX campaign in Mace Head,
55 Ireland, (Heard et al., 2006), following several studies which attributed box model overestimates of HO₂
56 observations in marine environments to unmeasured halogen monoxides (Carslaw et al., 1999; Carslaw et al.,
57 2002; Kanaya et al., 2001; Kanaya et al., 2002; Kanaya et al., 2007). Simultaneous measurements of OH and HO₂
58 by laser-induced fluorescence (LIF) (Bloss et al., 2005a; Smith et al., 2006) and halogen species by a combination
59 of DOAS (for BrO or IO, OIO and I₂) (Saiz-Lopez et al., 2006) and broadband cavity ringdown spectroscopy
60 (BCCRDS) (for OIO and I₂) (Bitter et al., 2005) during NAMBLEX enabled box model calculations to fully
61 explore the impacts of halogens on the local composition. A box model without halogen chemistry was able to
62 reproduce the NAMBLEX OH observations to within 25 %, but HO₂ observations were overestimated by up to a
63 factor of 2 (Sommariva et al., 2006). The introduction of halogen chemistry, using DOAS measurements of BrO
64 and IO (Saiz-Lopez et al., 2006) to constrain the model, increased the modelled OH concentrations by up to 15
65 % and decreased HO₂ by up to 30 % owing to reactions of HO₂ with XO radicals to form HOX which subsequently
66 photolysed to X + OH (Sommariva et al., 2006). Bloss et al., (2005a) indicated that up to 40 % of the instantaneous
67 HO₂ loss could be attributed to HO₂ + IO, and that photolysis of HOI was responsible for 15 % of the noontime
68 OH production.



69 The impacts of halogen chemistry on HO_x radicals at a site representative of the open ocean have been investigated
70 at the Cape Verde Atmospheric Observatory (CVAO). Measurements of halogen monoxides (Mahajan et al.,
71 2010a) at the site have been shown to have significant impacts on local ozone concentrations, notably in the
72 magnitude of the daily cycle (Read et al., 2008), and have been used to constrain box model calculations used to
73 explore observations of OH and HO₂ made during the RHaMBLe campaign in 2007 (Whalley et al., 2010). The
74 model calculations showed generally good comparisons with the observed OH and HO₂ concentrations, apart
75 from a period characterised by unusually high concentrations of HCHO. Compared to a model run in which
76 halogen chemistry was absent, bromine and iodine chemistry led to a 9 % increase in the modelled OH
77 concentration (Whalley et al., 2010). Owing to the dominance of the tropics in global methane oxidation (Bloss
78 et al., 2005b), such an impact of halogens on OH could have significant consequences for estimates of global
79 methane lifetimes, and on our understanding of the impacts of halogen chemistry on climate change.

80
81 In general, observationally constrained box model simulations suggest that halogens in the troposphere chemistry
82 will increase OH concentrations, primarily because of a change in the HO₂ to OH ratio occurring as a result of
83 reactions of halogen oxides (XO) with HO₂ to produce a hypohalous acid (HOX) which photolyses to give an OH
84 radical and a halogen atom (Kanaya et al., 2002; Bloss et al., 2005a; Kanaya et al., 2007; Sommariva et al., 2006;
85 Sommariva et al., 2007; Whalley et al., 2010). Other impacts on the HO_x photochemical system are observed
86 (impacts from changes to NO_x chemistry etc.) but these are minor and overall the general conclusion is that the
87 halogen chemistry tends to increase the OH concentration and thus the oxidising capacity of the atmosphere.

88
89 However, the observationally constrained studies are typically concerned with processes occurring at the surface,
90 and in a single location. The role of halogen chemistry in the troposphere as a whole is more uncertain, particularly
91 in the free troposphere and on a global scale (Saiz-Lopez and von Glasow, 2012; Simpson et al., 2015). Inclusion
92 of bromine chemistry in the three-dimensional (3D) chemistry transport model (CTM) MATCH-HPIC resulted
93 in decreases in tropospheric ozone concentrations of ~18 % over widespread areas, with regional decreases of up
94 to 40 % (von Glasow et al., 2004). Increases of more than 20 % were found for OH in the free troposphere, but,
95 globally, changes to OH were dominated by decreases in OH in the tropics owing to a reduction in primary
96 production from O₃ photolysis, leading to a decrease of 1-2 % in the global mean OH concentration (von Glasow
97 et al., 2004).

98
99 Significant decreases in tropospheric ozone (up to 30% at high latitude spring) were also reported for the
100 pTOMCAT model on inclusion of bromine chemistry (Yang et al., 2005). The CAM-Chem global chemistry-
101 climate model has shown an approximate 10 % decrease in global mean tropospheric ozone concentration on



102 incorporation of lower bromine emissions (Saiz-Lopez et al., 2012), while the GEOS-Chem CTM displays a
103 global decrease of 6.5 % (Parrella et al., 2012). The GEOS-Chem model indicated that bromine-catalysed loss
104 of ozone is limited by the rate of production of HOBr, and that HO₂ + BrO is responsible for over 95 % of the
105 global tropospheric HOBr production. While HOBr can act as a source of OH on photolysis, the changes to O₃
106 and NO_x resulting from the inclusion of bromine chemistry in GEOS-Chem led to a 4 % decrease overall in the
107 global annual mean OH (Parrella et al., 2012).

108
109 Vertically resolved airborne measurements of IO radicals in the free troposphere over the Pacific Ocean have also
110 demonstrated a role for iodine chemistry throughout the free troposphere, with IO observed at a mixing ratio of
111 ~0.1 ppt in the free troposphere and found to be present in both recent deep convective outflow and aged free
112 tropospheric air (Dix et al., 2013). Model simulations to investigate iodine-driven ozone destruction throughout
113 the troposphere indicated that only 34 % of the total iodine-driven ozone loss occurs within the marine boundary
114 layer, with 40 % occurring in a transition layer and 26 % in the free troposphere (Dix et al., 2013).

115
116 The CAM-Chem and GEOS-Chem models have also been updated to encompass iodine chemistry, with results
117 from CAM-Chem showing iodine chemistry to be responsible for 17-27 % of the ozone loss in the tropical MBL
118 and 11-27 % of the ozone loss in the marine upper troposphere (Saiz-Lopez et al., 2014). The GEOS-Chem model
119 also showed iodine chemistry to be responsible for significant ozone destruction throughout the troposphere
120 (Sherwen et al., 2016a; Sherwen et al., 2016b; Sherwen et al., 2017). The GEOS-Chem simulations, which
121 incorporate chlorine, bromine and iodine chemistry, show a reduction in global tropospheric ozone concentration
122 of 18.6 %, compared to simulations with no halogen chemistry, a reduction in the global mean OH of 8.2 % to a
123 concentration of $1.28 \times 10^6 \text{ cm}^{-3}$ and a resulting increase in global methane lifetime of 10.8 % to 8.28 years
124 (Sherwen et al., 2016b).

125
126 There is thus a discrepancy between box and global models as to the impact of halogen chemistry on OH
127 concentrations in the troposphere. Box models suggesting that OH radical concentrations should increase and
128 thus that halogens tend to increase the oxidising capacity, whereas the global models tend to suggest the opposite.

129
130 In this work, we use both a detailed chemical box model approach and a global chemistry-transport model to
131 investigate the local and global impacts of halogen chemistry on HO_x radical concentrations. We focus on
132 seasonal HO_x observations available from the Cape Verde Atmospheric Observatory (Vaughan et al., 2012). We
133 first provide a summary of the measurement site and the observations, followed by details of the two models used



134 in this study. We then evaluate the impact of halogens on the concentrations of oxidants in the two modelling
135 frameworks and consider the impact of halogen chemistry on global oxidising capacity.

136

137 **The Cape Verde Atmospheric Observatory**

138 The Cape Verde Atmospheric Observatory is situated on the north east coast of the island of Sao Vicente (16.848
139 °N, 24.871 °W), approximately 500 km off the west coast of Africa. The observatory is in a region of high marine
140 biological production, and, for 95 % of the time, receives the prevailing northeasterly trade wind directly off the
141 ocean (Read et al., 2008; Carpenter et al., 2010). Measurements at the observatory are considered to be
142 representative of the open ocean, and CO, O₃, VOCs, NO_x and NO_y have been measured near-continuously at the
143 observatory since October 2006 (Lee et al., 2009; Carpenter et al., 2010).

144

145 In 2007, the observatory was host to the RHaMBLe intensive field campaign, during which a number of additional
146 measurements were made to complement the long-term measurements at the site (Lee et al., 2010), including LP-
147 DOAS measurements of halogen species (Read et al., 2008; Mahajan et al., 2010a) and formaldehyde (Mahajan
148 et al., 2010b), and LIF-FAGE measurements of OH and HO₂ (Whalley et al., 2010). The halogen monooxide
149 radicals BrO and IO exhibited a ‘top-hat’ diurnal cycle (Vogt et al., 1999; Vogt et al., 1996; Read et al., 2008;
150 Mahajan et al., 2010a) with essentially zero concentration in the hours of darkness and generally constant values
151 of approximately 2.5 ppt BrO and 1.4 ppt IO during the day.

152

153 The RHaMBLe campaign was followed by the Seasonal Oxidants Study (SOS) in 2009, during which
154 measurements of OH and HO₂ were conducted over three periods (Feb-March (SOS1), May-June (SOS2), and
155 September (SOS3)), and are discussed in detail by Vaughan et al. (2012). We present here the results from a
156 modelling study of the HO_x measurements made during SOS1 and SOS2, when supporting measurements are
157 available, using both box and global model approaches. SOS3 is not considered in this work owing to a lack of
158 supporting measurements.

159

160 Measurements of OH and HO₂ during the Seasonal Oxidant Study were made by laser-induced fluorescence (LIF)
161 spectroscopy at low pressure using the fluorescence assay by gas expansion (FAGE) technique, and are described
162 in detail by Vaughan et al. (2012). Briefly, ambient air is drawn into a fluorescence cell situated on the roof of a
163 shipping container and maintained at pressures of ~ 2 Torr. The fluorescence cell has two excitation axes, with
164 excess NO added at the second axis to titrate HO₂ to OH, enabling simultaneous detection of OH and HO₂. OH
165 radicals in both excitation axes are excited by laser light at $\lambda \sim 308$ nm, generated by frequency tripling the output



166 of a solid state Nd:YAG pumped Ti:Sapphire laser system (Bloss et al., 2003). Channel photomultiplier tubes
167 coupled to gated photon counters are used to detect the $A^2\Sigma^+ - X^2\Pi_i$ OH fluorescence signal at $\lambda \sim 308$ nm.

168
169 Calibration of the instrument is achieved by measurement of the fluorescence signal from known concentrations
170 of OH and HO₂, produced by the photolysis of water vapour, and was performed over a range of conditions before,
171 during and after the campaign. For OH, the 1 σ limit of detection (LOD) was in the range $(2-11) \times 10^5$ cm⁻³ for a
172 5 min averaging period, while for HO₂ 1 σ LOD was in the range $(6-13) \times 10^5$ cm⁻³ for a 4 min averaging period.
173 Uncertainties (2 σ) in the measurements of OH and HO₂ are ~ 32 % (Vaughan et al., 2012).

174
175 Potential interferences in HO₂ measurements arising from conversion of alkene- and aromatic-derived peroxy
176 radicals to OH within the LIF detection cell, as described by Fuchs et al. (2011), are expected to be small for this
177 work owing to relatively low concentrations of alkenes and aromatics at the Cape Verde observatory (Carpenter
178 et al., 2010; Vaughan et al., 2012). Speciation of the peroxy radicals in the box model output (see Supplementary
179 Material) shows that 87.4 % of the peroxy radicals are HO₂ and CH₃O₂, 6.5 % CH₃C(O)O₂ and 1.1 % C₂H₅O₂,
180 all of which display no HO₂ interference in the laboratory (Whalley et al., 2013; Stone et al., 2014). Peroxy
181 radicals derived from OH-initiated oxidation of ethene and propene (HOC₂H₄O₂ and HOC₃H₆O₂, respectively)
182 were found to result in an interference signal for HO₂ in the laboratory (~ 40 % for the experimental configuration
183 in this work) but each radical comprises only ~ 0.6 % of the total RO₂ in this work. Thus, model calculations
184 reported here do not include representation of potential HO₂ interferences, although such phenomena may be
185 important in other environments (see for example, Whalley et al., 2013; Stone et al., 2014).

186

187 **Model Approaches**

188 We interpret the observations using two different modeling frameworks. The first is an observationally
189 constrained box model (DSMACC), the second is a global tropospheric chemistry transport model (GEOS-
190 Chem).

191

192 **Constrained Box Model**

193 The Dynamically Simple Model of Atmospheric Chemical Complexity (DSMACC) is described in detail by
194 Emmerson and Evans (2009) and Stone et al. (2010), and is a zero-dimensional model using the Kinetic Pre-
195 Processor (KPP) (Sandu and Sander, 2006). In this work we use a chemistry scheme based on a subsection of the
196 hydrocarbons (ethane, propane, *iso*-butane, *n*-butane, *iso*-pentane, *n*-pentane, hexane, ethene, propene, 1-butene,
197 acetylene, isoprene, toluene, benzene, methanol, acetone, acetaldehyde and DMS) available from the Master
198 Chemical Mechanism version 3.2 (MCM v3.2 <http://mcm.leeds.ac.uk/MCM/home.htm>) (Jenkin et al., 2003;



199 Saunders et al., 2003), with a halogen chemistry scheme described by Saiz-Lopez et al. (2006), Whalley et al.
200 (2010) and Edwards et al. (2011). We also include the reaction between OH and CH₃O₂ (Bossolasco et al., 2014;
201 Fittschen et al., 2014; Assaf et al., 2016; Yan et al., 2016), with a rate coefficient of $1.6 \times 10^{-10} \text{ cm}^3 \text{ s}^{-1}$ (Assaf et
202 al., 2016) and products HO₂ + CH₃O (Assaf et al., 2017), the impact of which on the HO₂:OH ratio and CH₃O₂
203 budget is described in the Supplementary Material. The total number of species in the model is ~1200, with ~5000
204 reactions. The full chemistry scheme used in the model is given in the Supplementary Data.

205
206 All measurements are merged onto a 10 minute timebase for input to the model and the model is run with
207 constraints applied as discussed in our previous work (Stone et al., 2010; Stone et al., 2011; Stone et al., 2014).
208 Concentrations of CH₄ and H₂ are kept constant at values of 1770 ppb (NOAA CMDL flask analysis,
209 <ftp://ftp.cmdl.noaa.gov/ccg/ch4/>) and 550 ppb (Ehhalt and Rohrer, 2009; Novelli et al., 1999) respectively.
210 Formaldehyde measurements were not available during the SOS and we thus use HCHO concentrations generated
211 by the chemistry in the model, with the modelled HCHO concentrations in broad agreement with previous
212 measurements at the observatory (Mahajan et al., 2010b). Table 1 shows a summary of the input parameters to
213 the model.



Species	Mean	Median	Range
O₃ / ppb	33.8 ± 8.6	30.7	19.6 – 49.7
CO / ppb	102.3 ± 10.3	99.3	87.8 – 127.3
H₂O / ppm	20542.3 ± 2753.8	21290.0	16778.5 – 24909.2
NO / ppt	11.2 ± 10.6	9.0	0.06 – 96.2
Ethane / ppt	961.3 ± 289.4	864.0	625.4 – 1799.2
Propane / ppt	136.1 ± 87.05	111.8	20.2 – 521.5
<i>iso</i> -butane / ppt	13.4 ± 9.8	11.1	0 – 62.7
<i>n</i> -butane / ppt	21.9 ± 17.6	17.8	0 – 112.9
Acetylene / ppt	79.0 ± 27.8	70.4	45.0 – 180.5
Isoprene / ppt	0.1 ± 0.4	0	0 – 2.6
<i>iso</i> -pentane / ppt	3.9 ± 3.2	3.3	0 – 22.9
<i>n</i> -pentane / ppt	4.3 ± 3.0	3.9	0 – 21.7
<i>n</i> -hexane / ppt	1.0 ± 0.7	0.9	0 – 4.4
Ethene / ppt	43.6 ± 15.2	46.3	6.4 – 73.2
Propene / ppt	13.5 ± 3.6	13.0	6.2 – 24.1
But-1-ene / ppt	6.5 ± 1.4	6.3	3.5 – 10.6
Benzene / ppt	13.0 ± 17.0	8.3	0 – 64.4
Toluene / ppt	77.9 ± 388.8	0	0 – 2013.9
Acetaldehyde / ppt	511.8 ± 526.0	599.3	0 – 2622.6
Methanol / ppt	247.6 ± 336.2	173.3	0 – 3337.4
DMS / ppt	8.3 ± 38.3	0	0 – 291.8

214 Table 1: Summary of inputs to the model. Zero values indicate measurements below the limit of detection.

215 Further details can be found in Vaughan et al. (2012) and Carpenter et al. (2010).

216

217

218

219

220

221

222

223



224 Physical loss of each species in the model is represented by a first-order loss process, with the first-order rate
225 coefficient equivalent to a lifetime of approximately 24 hours, as discussed by Stone et al. (2010). Loss of reactive
226 species to aerosol surfaces is represented in the model by parameterisation of a first-order loss process to the
227 aerosol surface (Schwarz, 1986), as discussed by Stone et al. (2014).

228
229 A range of aerosol uptake coefficients for HO₂ have been reported in the literature, with recent measurements
230 indicating values of γ_{HO_2} between 0.003 and 0.02 on aqueous aerosols (George et al., 2013) while others have
231 reported values of $\gamma_{\text{HO}_2} \sim 0.1$ (Taketani et al., 2008), and increased uptake coefficients in the presence of Cu and
232 Fe ions (Thornton et al., 2008; Mao et al., 2013). In this work we use a value of $\gamma_{\text{HO}_2} = 0.1$ in order to maintain
233 consistency with previous modelling studies at the site (Whalley et al., 2010) and to account for potential impacts
234 of ions of copper and iron in aerosol particles influenced by mineral dust (Carpenter et al., 2010; Muller et al.,
235 2010; Fomba et al., 2014; Matthews et al., 2014; Lakey et al., 2015).

236
237 The aerosol surface area in the model is constrained to previous measurements of dry aerosol surface area at the
238 observatory, corrected for differences in sampling height between the aerosol and HO_x measurements and for
239 aerosol growth under humid conditions (Allan et al., 2009; Muller et al., 2010; Whalley et al., 2010).

240
241 Halogen species are constrained to a ‘top-hat’ profiles for BrO and IO (Vogt et al., 1999; Vogt et al., 1996; Read
242 et al., 2008), as observed during the RHAMBLE campaign in 2007 (Read et al., 2008; Mahajan et al., 2010a).
243 The observations indicate that while there is day to day variation in BrO and IO concentrations, there is little
244 seasonal variation (Mahajan et al., 2010a). BrO and IO are thus constrained to the mean observed mixing ratios
245 of 2.5 ppt and 1.4 ppt, respectively, for time points between 0930 and 1830 (GMT) and zero for all other times.
246 In a similar way to NO_x (see Stone et al. (2010; 2011)), concentrations of all bromine or iodine species, including
247 BrO and IO, are permitted to vary according to the photochemistry as the model runs forwards. At the end of
248 each 24 hour period in the model, the calculated concentrations of BrO and IO are compared to the constrained
249 value, and the concentrations of all bromine (Br, Br₂, BrO, HBr, HOBr, BrONO₂, BrNO₂, BrNO) and iodine (I,
250 I₂, IO, HI, HOI, INO, INO₂, IONO₂, OIO, I₂O₂, I₂O₃, I₂O₄, HOIO₂) species are fractionally increased or decreased
251 such that the calculated and constrained concentrations of BrO and IO are the same. The model is run forwards
252 in time with diurnally varying photolysis rates until a diurnal steady state is reached, typically requiring between
253 5 and 10 days.

254

255

256



257 **Global Model**

258 We use the 3D global chemistry transport model GEOS-Chem (v10-01, www.geos-chem.org). The model has
259 been extensively evaluated against observations (Bey et al., 2001; Evans and Jacob, 2005; Nassar et al., 2009;
260 Mao et al., 2010; Zhang et al., 2010; Parrella et al., 2012; Hu et al., 2017). The model is driven by assimilated
261 winds calculated by the Goddard Earth Observing System at a horizontal resolution of $4^\circ \times 5^\circ$, with 47 vertical
262 levels from the surface to 50 hPa. Anthropogenic emissions of CO, NO_x and SO₂ are described by the EDGAR
263 3.2 monthly global inventory (Olivier et al., 2005). Emissions of volatile organic compounds (VOCs) are
264 described by the RETRO monthly global inventory (van het Bolscher, 2008) for anthropogenic sources, with
265 ethane emissions described by Xiao et al., 2008, and the MEGAN v2.1 inventory (Guenther et al., 2006; Barkley
266 et al., 2011) for biogenic sources.

267
268 The HO_x-NO_x-VOC-O₃ chemistry scheme in the model is described in detail by Bey et al. (2001) and Mao et al.
269 (2013), with the isoprene oxidation mechanism described by Paulot et al. (2009). Photolysis rates use the FAST-
270 JX scheme (Bian and Prather, 2002; Mao et al., 2010), with acetone photolysis rates updated by Fischer et al.
271 (2012). Stratospheric chemistry is based on LINOZ McLinden et al. (2000) for O₃ and a linearised mechanism
272 for other species as described by Murray et al. (2012).

273
274 The model framework includes gas-aerosol partitioning of semi-volatile organic compounds (Liao et al., 2007;
275 Henze et al., 2007; Henze et al., 2009; Fu et al., 2008; Heald et al., 2011; Wang et al., 2011), and heterogeneous
276 chemistry (Jacob, 2000). Coupling between gas phase chemistry and sulfate-ammonium-nitrate aerosol is
277 described by Park et al. (2004) and Pye et al. (2009). A description of dust aerosol in the model is given by Fairlie
278 et al. (2007). Treatment of sea salt aerosol is described by Jaegle et al. (2011). The uptake coefficient for N₂O₅
279 uses the parameterisation by Evans and Jacob (2005), while that for HO₂ uses the parameterisation of Thornton
280 et al. (2008). A full description of the organic aerosol chemistry in the model is given by Heald et al. (2011).

281
282 The model includes recent updates to the chemistry scheme to include bromine chemistry (Parella et al., 2012;
283 Schmidt et al., 2016) and iodine chemistry (Sherwen et al., 2016a; Sherwen et al., 2016b). Sources of tropospheric
284 bromine in the model include emissions of CHBr₃, CH₂Br₂ and CH₃Br, and transport of reactive bromine from
285 the stratosphere. Debromination of sea-salt aerosol is not included in the model following the work of Schmidt et
286 al. (2016), which showed better agreement with observations of BrO made by the GOME-2 satellite (Theys et al.,
287 2011) and in the free troposphere and the tropical Eastern Pacific MBL (Gomez Martin et al., 2013; Volkamer et
288 al., 2015; Wang et al., 2015). Emission rates and bromine chemistry included in the model are described in detail
289 by Parella et al. (2012), with the additional bromine chemistry scheme described by 19 bimolecular reactions, 2



290 three-body reactions and 2 heterogeneous reactions using rate coefficients, heterogeneous reaction coefficients
291 and photolysis cross-sections recommended by Sander et al. (2011).

292
293 Iodine sources include emissions of CH_3I , CH_2I_2 , CH_2ICl , CH_2IBr , I_2 and HOI . Emissions for CH_3I follow Bell
294 et al. (2002), while those of other organic iodine species use parameterisations based on chlorophyll-a in the
295 Tropics and constant oceanic and coastal fluxes in extratropical regions (Ordonez et al., 2012). Emissions of
296 inorganic iodine species (HOI and I_2) use the results of Carpenter et al. (2013), with oceanic iodide concentrations
297 parameterised by MacDonald et al. (2014). The iodine chemistry scheme includes 26 unimolecular and
298 bimolecular reactions, 3 three-body reactions, 21 photolysis reactions and 7 heterogeneous reactions, using
299 recommendations by Atkinson et al. (2007) and Sander et al. (2011) where available. Full details are given by
300 Sherwen et al. (2016a; 2016b).

301
302 Photolysis rates of bromine and iodine compounds are calculated using the FAST-J radiative transfer model (Wild
303 et al., 2000; Bian and Prather, 2002; Mao et al., 2010). Wet and dry deposition are determined as for the standard
304 GEOS-Chem model (Liu et al., 2001; Wesely, 1989; Wang et al., 1998; Amos et al., 2012).

305
306 The tropospheric chemistry scheme is integrated using the SMVGEAR solver (Jacobson and Turco, 1994; Bey et
307 al., 2001). The model, provides hourly output at the site of the Cape Verde Atmospheric Observatory. Model
308 simulations have been performed in the absence of halogens, with bromine chemistry, with iodine chemistry and
309 with bromine and iodine chemistry combined. Each model simulation is run for two years, with the analysis
310 performed on the second year (2009) and the first year discarded as model spin-up to enable evolution of long-
311 lived species.

312
313 **Model Results**
314 We now investigate the impact of halogen chemistry on tropospheric oxidation at Cape Verde within our two
315 modelling approaches.

316
317 **Constrained Box Model**
318 Figure 1 shows the observed and modelled time series for OH and HO_2 during SOS1 (February, March 2009) and
319 SOS2 (May, June 2009). Observed concentrations of OH and HO_2 were typically higher in SOS2 than SOS1,
320 reaching maximum values in SOS2 of $\sim 9 \times 10^6 \text{ cm}^{-3}$ OH and $4 \times 10^8 \text{ cm}^{-3}$ HO_2 (Vaughan et al., 2012). Similar
321 concentrations were observed in May and June 2007 during the RHAMBLE campaign (Whalley et al., 2010), with
322 a *t*-test indicating no statistically significant difference between the OH concentrations measured in May-June



323 2009 to those measured in May-June 2007 at the 95 % confidence level (Vaughan et al., 2012). Concentrations
324 of HO₂ measured in May-June 2009 were significantly higher than those measured in May-June 2007 at the 95
325 % confidence level, but were within the 1σ day-to-day variability (Vaughan et al., 2012). Temperatures during
326 SOS2 were typically higher than those during SOS1, with higher relative humidity during SOS2 (Vaughan et al.,
327 2012). Air masses during SOS1 had strong contributions from Atlantic marine air and African coastal region,
328 with polluted marine air and Saharan dust contributing ~ 20 % and 10 %, respectively, for the first half of the
329 measurement period. Conditions during SOS2 were typically cleaner, with Atlantic marine air representing the
330 major source, although coastal African air contributed ~ 40 % on some days. There was little influence from
331 polluted air, dust or continental air (Vaughan et al., 2012). Analysis of the variance of OH and HO₂ during SOS
332 indicated that ~70 % of the total variance could be explained by diurnal behaviour, with the remaining ~30 %
333 related to changes in air mass.

334
335 Figure 1 shows the observed and modelled time series for OH and HO₂, for model simulations with and without
336 halogen chemistry. For SOS1, the box model overpredicts the OH and HO₂ concentrations at the start of the
337 campaign (Julian days 59 and 61), but performs better for day 63, and captures both the observed diurnal profile
338 and the observed concentrations. For SOS2, the box model tends to agree better with the observations for both
339 OH and HO₂. A day-by-day comparison between the models and the observations is shown in the Supplementary
340 Material for days for which box model calculations were possible, which were limited by the availability of
341 supporting data.

342
343 Figure 2 shows the point-by-point model performance for OH and HO₂ for all data points combined, and for
344 SOS1 and SOS2 separately, for the full box model run including halogen chemistry. There is a tendency for
345 overprediction of OH and HO₂ during SOS1 (slopes of modelled vs observed concentrations are (1.86 ± 0.26) for
346 OH and (1.66 ± 0.21) for HO₂), which is dominated by the model overpredictions on days 59 and 61, with better
347 agreement observed during SOS2 (slopes of modelled vs observed concentrations are (1.11 ± 0.15) for OH and
348 (1.21 ± 0.12) for HO₂).

349
350 The measured and modelled average diurnal profiles of OH, HO₂ and the HO₂ to OH ratios are shown in Figure
351 3. At midday (1100-1300), the full model including halogen chemistry overpredicts OH by a median factor of
352 1.52 and HO₂ by a median factor of 1.21. A model run containing bromine chemistry but no iodine chemistry
353 gave median midday overpredictions of 1.40 and 1.30 for OH and HO₂, respectively, while a run containing
354 iodine but not bromine gave equivalent median overpredictions of 1.50 and 1.26, respectively. With no halogen
355 chemistry included in the model, the modelled OH decreases, giving a median overprediction at midday by a



356 factor of 1.37, while the modelled HO₂ increases, resulting in a median overprediction by a factor of 1.37 at
357 midday.

358
359 Thus the inclusion of halogens (bromine and iodine) in the box model changes the mean noon time OH and HO₂
360 concentrations by +9.8 % and -9.9 %, respectively. This impact of halogen chemistry is consistent in sign and
361 magnitude with previous studies (Kanaya et al., 2002; Bloss et al., 2005a; Kanaya et al., 2007; Sommariva et al.,
362 2006; Sommariva et al., 2007; Whalley et al., 2010).

363
364 Figure 4 shows the mean midday total RO_x budget (given the fast processing time between HO₂ and HOBr/HOI
365 we identify the RO_x family as OH, HO₂, HOBr, HOI, RO and RO₂) for the two measurement periods during SOS
366 for model runs with and without halogens. These budgets are similar both between time periods (i.e. SOS1 vs
367 SOS2) and for box model calculations with and without halogen chemistry. Radical production dominated by
368 photolysis of ozone (~83 %), with photolysis of HCHO (~10 %), CH₃CHO (~2 %) and H₂O₂ (~2 %) playing a
369 significantly smaller role. Radical termination reactions were dominated by HO₂ + CH₃O₂ (~23 %), aerosol uptake
370 of HO₂ (~21 %), HO₂ + HO₂ (~19 %), CH₃C(O)O₂ + HO₂ (~8 %), and OH + HO₂ (~5 %). The inclusion of the
371 reaction between OH and CH₃O₂ reduces the importance of radical termination via HO₂ + CH₃O₂ (from ~26 %
372 of the total to ~23 % of the total), but otherwise has little impact on the total radical removal owing to the expected
373 production of HO₂ + CH₃O (Assaf et al., 2017). Further details regarding the impact of the reaction between OH
374 and CH₃O₂ on the HO₂:OH ratio and CH₃O₂ budget are given in the Supplementary Material.

375
376 The budget analyses for SOS are consistent with those determined for the RHaMBLe campaign (Whalley et al.,
377 2010; Fittschen et al., 2014; Assaf et al., 2017), reflecting similarities in observed concentrations of long-lived
378 species and the method of the model constraint with observed O₃ concentrations and photolysis rates. The primary
379 source of radicals therefore remains fixed in all simulations, with the primary sinks for these species occurring
380 through radical-radical reactions. Thus, the total radical concentration and budget is little impacted by the
381 presence of halogens.

382
383 However, the partitioning of the radicals is impacted by the halogens. Without halogens the average midday
384 (1100-1300) HO₂ to OH ratio is (83.4 ± 15.4) (median = 82.7), with the halogens this changes to (68.3 ± 13.6)
385 (median = 66.9) (Table 2). This change in partitioning is mainly due to the reaction of HO₂ with BrO and IO
386 followed by the photolysis of HOBr and HOI to give OH. In this way the halogens tend to reduce the concentration
387 of HO₂ and increase the concentration of OH.

388



	HO ₂ :OH ratio
Observed	79.1 ± 34.1 (70.7)
Box model, no halogens	83.4 ± 15.4 (82.7)
Box model with Br chemistry	78.9 ± 15.6 (77.8)
Box model with I chemistry	71.5 ± 13.0 (70.4)
Box model with Br and I chemistry	68.3 ± 13.6 (66.9)
Global model, no halogens	80.8 ± 18.1 (78.9)
Global model with Br chemistry	81.9 ± 19.0 (79.7)
Global model with I chemistry	70.4 ± 12.5 (70.5)
Global model with Br and I chemistry	71.3 ± 13.2 (71.3)

389

390 Table 2: Mean ($\pm 1\sigma$) midday (1100-1300 hours) ratios of HO₂ to OH (SOS1 and SOS2 combined). Median
 391 values are given in parentheses.

392

393 In the box model without halogen chemistry, production of OH is dominated by ozone photolysis (76 %), HO₂ +
 394 NO (12 %) and HO₂ + O₃ (9 %), with OH loss controlled by OH + CO (37 %), OH + CH₄ (16 %) and OH +
 395 CH₃CHO (15 %), as shown in Figure 5. Production of HO₂ in the model excluding halogens is controlled by OH
 396 + CO (45 %), CH₃O + O₂ (19 %) and photolysis of HCHO (10 %), with loss governed by aerosol uptake (26 %),
 397 HO₂ + HO₂ (26 %), HO₂ + NO (15 %), HO₂ + CH₃O₂ (12 %) and HO₂ + O₃ (10 %). In the presence of halogens,
 398 the instantaneous budgets for OH and HO₂ are impacted by BrO and IO, as shown in Figures 5 and 6. For the
 399 model run including halogens, OH production is still dominated by ozone photolysis (68 %), but there are
 400 significant contributions from photolysis of HOI (10 %) and HOBr (3 %). Loss of HO₂ is also affected by the
 401 presence of the halogen species, with the dominant loss processes including aerosol uptake (20 %), HO₂ + HO₂
 402 (19 %), HO₂ + IO (14 %), HO₂ + NO (12 %), HO₂ + CH₃O₂ (11 %), HO₂ + O₃ (8 %) and HO₂ + BrO (6 %). As
 403 shown in Figures 4-6 there is little difference in the radical budgets between SOS1 and SOS2.

404

405 This box modelling study is consistent with previous studies (Kanaya et al., 2002; Bloss et al., 2005a; Kanaya et
 406 al., 2007; Sommariva et al., 2007; Whalley et al., 2010; Mahajan et al., 2010a; Stone et al., 2012) in that it implies
 407 that halogen chemistry is likely to increase the OH concentration of the marine boundary layer (and potentially
 408 other regions of the troposphere) as it enhances the HO₂ to OH conversion through the production of HOBr and
 409 HOI. We now look at the impact of halogen chemistry on the concentrations of OH and HO₂ at Cape Verde within
 410 the framework of a global atmospheric chemistry model.

411

412



413 **Global Model**

414 Figure 1 shows the time series for OH and HO₂ calculated by the global model GEOS-Chem, with the average
415 diurnal profiles shown in Figure 3. The global model displays a significant overprediction for OH and HO₂ during
416 SOS1, but exhibits reasonable skill at reproducing the observed concentrations during SOS2 and captures the
417 HO₂:OH ratio for both measurement periods. The overpredictions of OH and HO₂ in the global model likely result
418 from a combination of missing OH-sinks, particularly oxygenated volatile organic compounds (oVOCs) which
419 are currently underestimated in the global model (Millet et al., 2015), and potential overprediction of the primary
420 radical production rate owing to reductions in photolysis rates resulting from cloud cover that are not captured by
421 the global model.

422
423 At midday (1100-1300), the modelled to observed ratios for OH and HO₂ for the global model excluding halogen
424 chemistry are (1.52 ± 1.02) and (1.72 ± 0.80), respectively, with a mean modelled HO₂ to OH ratio of (80.8 ±
425 18.1) (compared to the observed HO₂ to OH ratio of (79.1 ± 34.1)). For the global model run including bromine
426 chemistry, but not iodine, the mean midday modelled to observed ratios for OH and HO₂ are (1.48 ± 1.05) and
427 (1.69 ± 0.81), respectively, with a mean midday modelled HO₂ to OH ratio of (81.9 ± 19.0). Bromine chemistry
428 thus acts to decrease the concentrations of both OH and HO₂, in contrast to the box model results which show
429 increased concentrations of OH and decreased concentrations of HO₂. For the model run including iodine, but not
430 bromine, the midday modelled to observed ratios for OH and HO₂ are (1.57 ± 1.00) and (1.59 ± 0.81), respectively,
431 with a mean midday modelled HO₂ to OH ratio of (70.4 ± 12.5). Iodine chemistry thus results in increased OH
432 and decreased HO₂ for both the global and box model simulations at Cape Verde. Inclusion of bromine and iodine
433 chemistry combined leads to midday modelled to observed ratios of (1.53 ± 1.01) for OH and (1.57 ± 0.82) for
434 HO₂, and a mean midday modelled HO₂ to OH ratio of (71.3 ± 13.2). These results are shown in Table 2, alongside
435 those for the box model.

436
437 The results from the global model at Cape Verde thus differ from those of the box model. For the box model,
438 inclusion of bromine and iodine chemistry, whether separately or combined, leads to increased OH and decreased
439 HO₂ through increased conversion of HO₂ to OH through the production and subsequent photolysis of HOBr and
440 HOI. In the global model a more complex pattern emerges. In a similar way to the box model, the HO₂
441 concentrations in the global model are decreased on inclusion of bromine and/or iodine owing to the additional
442 loss reactions HO₂ + BrO and HO₂ + IO. When bromine chemistry is considered in the global model in isolation
443 from iodine chemistry, the OH concentration decreases, despite the production and photolysis of HOBr. This
444 decrease occurs as a result of a reduction in the O₃ concentration in the model on inclusion of bromine chemistry
445 owing to the reaction of Br with O₃, which leads to a decrease in the rate of primary radical production from O₃



446 photolysis and thus lower OH concentrations. The impact of the decreased radical production rate is greater than
447 that leading to increased OH production through HOBr photolysis, and the net OH concentration is reduced in
448 the global model. This effect is not observed in the box model calculations as the model runs are constrained to
449 long-lived species – including O₃. The change in O₃ concentration on the inclusion of halogen chemistry is thus
450 not considered in the box model simulations, and the subsequent impacts of halogens consider only those changes
451 occurring on a more rapid timescale, which lead to increases in the OH concentration.

452
453 However, the inclusion of iodine chemistry in the global model does lead to increased OH concentrations at Cape
454 Verde. Direct emissions of HOI in the global model, in addition to chemical production through HO₂ + IO, result
455 in increased OH production through HOI photolysis as well as the repartitioning of HO₂ and OH through HOI
456 production in a similar manner to that for HOBr. However, the more rapid cycling of HO₂ to OH through the
457 more rapid production and photolysis of HOI compared to HOBr, reduces the impact of iodine chemistry on the
458 HO₂:OH ratio compared to that for bromine chemistry. Iodine chemistry thus can reduce the OH concentration
459 similarly to bromine chemistry, through the destruction of O₃ and subsequent reduction in primary production
460 rate, but the impact is less than that for bromine, and can be offset by the direct emissions of HOI which increases
461 the production rate of OH through photolysis.

462
463 The impacts of iodine chemistry in the global model are thus more complex than those for bromine chemistry.
464 When bromine and iodine chemistry are combined in the global model there is a competition between the effects
465 of the reduction in primary production of OH, through depletion of O₃, and the production of OH from photolysis
466 of HOBr and HOI and, for the model simulations at Cape Verde, the impacts of direct HOI emissions dominate.
467 The OH concentration is thus marginally increased compared to simulations containing no halogens, although the
468 HO₂ concentrations are significantly decreased.

469
470 The impacts of halogens on OH radical concentrations in the global model thus display a complexity that is
471 somewhat obscured in the box model simulations. Overall, the inclusion of halogens in the global model leads to
472 a slight increase in OH at Cape Verde, but, owing to the opposing effects of bromine and iodine, this result is
473 subject to the modelled concentrations of bromine and iodine species. Observations at Cape Verde made between
474 November 2006 and June 2007 indicate ‘top-hat’ profiles for BrO and IO, with average daytime mixing ratios of
475 2.5 ppt and 1.4 ppt, respectively, and little variability over the entire campaign (Read et al., 2008; Mahajan et al.,
476 2010a). The global model simulations reported here predict average mixing ratios of ~0.5 ppt for BrO and ~1 ppt
477 for IO during SOS, and thus underpredict BrO but perform well for IO. The underprediction of BrO at Cape Verde
478 results from recent model updates which exclude emissions of bromine species from sea-salt debromination



479 (Schmidt et al., 2016) in order to provide improved agreement with observations of BrO made by the GOME-2
480 satellite (Theys et al., 2011) and in the free troposphere and the tropical Eastern Pacific MBL (Gomez Martin et
481 al., 2013; Volkamer et al., 2015; Wang et al., 2015). We now discuss the global impacts of halogen chemistry.
482

483 **Global impacts of halogen chemistry on OH and HO₂**

484 On the global scale, concentrations of OH and HO₂ are reduced on inclusion of bromine and iodine chemistry,
485 both individually and combined. The global mass weighted annual mean OH concentration decreases by 3.8 %
486 on inclusion of bromine chemistry, but only 0.02 % on inclusion of iodine chemistry alone. When the chemistry
487 of bromine and iodine is combined in the model, the global mass weighted annual mean OH concentration
488 decreases by 4.5 %. For HO₂, the global mass weighted annual mean is decreased by 4.2 % by bromine, 5.6 % by
489 iodine and 9.7 % by bromine and iodine combined. Figure 7 shows the probability distribution functions for the
490 changes to OH and HO₂ concentrations for the monthly mean values for all grid boxes within the troposphere for
491 the year. For the majority of grid boxes, concentrations of OH and HO₂ are reduced on inclusion of bromine
492 chemistry, with iodine also generally reducing HO₂ concentrations but leading to a wider spread of changes to
493 the OH concentration, and similar numbers of grid boxes showing increased and decreased concentrations. When
494 bromine and iodine chemistry are combined in the model, HO₂ shows a more significant decrease than for either
495 halogen individually, and OH, although exhibiting increased concentrations in a significant number of grid boxes,
496 displays a greater tendency for decreased concentrations.

497
498 Figure 8 shows the changes to the annual modelled surface layer OH and HO₂ concentrations on inclusion of
499 halogen chemistry, with annual surface layer mixing ratios of BrO and IO shown in Figure 9. The most significant
500 changes to OH and HO₂ occur over marine regions, particularly over the Southern Pacific. Smaller changes are
501 observed over land, and any increased concentrations, including those for OH over Cape Verde, can be seen to
502 occur in coastal regions where the impacts of direct HOI emissions dominate and concentrations of IO
503 concentrations are typically elevated.

504
505 Thus, overall, halogens act to reduce the oxidising capacity of the troposphere through reductions to O₃ and
506 subsequent reductions in the primary production rates of OH and HO₂, despite the slight increase in OH
507 concentration predicted by the global model at Cape Verde. Consideration of the full extent of the impacts of
508 halogens on the global oxidising capacity is hindered by uncertainties in the concentrations and distributions of
509 halogen species, and model representations of halogen processes, particularly those relating to sea salt
510 debromination, ocean iodide emissions, parameterisations of iodine recycling in aerosols and photolysis of higher
511 iodine oxides (Sherwen et al., 2016a).



512 **Conclusions**

513 Measurements of OH and HO₂ made by LIF-FAGE at the Cape Verde Atmospheric Observatory during the
514 Seasonal Oxidants Study in 2009 have been simulated by a constrained box model and a three-dimensional global
515 chemistry transport model. The observations are generally reproduced well by the box model, but are
516 overpredicted by the global model.

517
518 The oxidising capacity of the two models, as manifested by the OH concentration, shows opposing sensitivity to
519 halogens. The constrained box model shows an increase in OH concentrations with the inclusion of halogens,
520 whereas the global transport model shows a decrease in OH concentrations globally, despite a marginal decrease
521 in the OH concentration at Cape Verde. This difference between models reflects differing representation of
522 chemical timescales by the models. The box model is constrained to concentrations of long-lived compounds,
523 including O₃, and considers only impacts on short timescales, whereas the global model includes impacts
524 occurring on longer timescales. Within this context, the box model includes the short timescale impact of halogens
525 on the repartitioning of HO₂ to OH, thus increasing OH and decreasing HO₂, but does not consider the longer
526 timescale impact of halogen-mediated ozone destruction which impacts primary radical production. This
527 highlights a general problem with understanding the complex interactions within atmospheric chemistry and the
528 Earth system in general. Evaluating the impact of a small part of the system on the system as a whole can be
529 difficult and the most significant processes may occur on timescales significantly longer than those of the
530 perturbation.

531

532 **Acknowledgements**

533 This project was funded by the Natural Environment Research Council (NERC, NE/E011403/1), with support of
534 the Cape Verde Atmospheric Observatory by the National Centre for Atmospheric Science (NCAS) and the
535 SOLAS project. DS would also like to thank NERC for the award of an Independent Research Fellowship
536 (NE/L010798/1). Computational resources were provided by the NERC BACCHUS project (NE/L01291X/1)

537

538 **References**

539 Alicke, B., Hebestriest, H., Stutz, J., Platt, U.: Iodine oxide in the marine boundary layer, *Nature*, 397, 572-573,
540 1999

541

542 Allan, J.D., Topping, D.O., Good, N., Irwin, M., Flynn, M., Williams, P.I., Coe, H., Baker, A.R., Martino, M.,
543 Niedermeier, N., Wiedensohler, A., Lehmann, S., Muller, K., Herrmann, H., and McFiggans, G.: Composition
544 and properties of atmospheric particles in the eastern Atlantic and impacts on gas phase uptake
545 rates, *Atmos. Chem. Phys.*, 9, 9299–9314, 2009



- 546
547 Amos, H.M., Jacob, D.J., Holmes, C.D., Fisher, J.A., Wang, Q., Yantosca, R.M., Corbitt, E.S., Galarneau, E.,
548 Rutter, A.P., Gustin, M.S., Steffen, A., Schauer, J.J., Graydon, J.A., St. Louis, V.L., Talbot, R.W., Edgerton, E.S.,
549 Zhang, Y., and Sunderland, E.M: Gas-particle partitioning of Hg(II) and its effect on global mercury deposition,
550 Atmos. Chem. Phys., 12, 1, 591-603, doi:10.5194/acp-12-591-2012, 2012
551
552 Assaf, E., Song, B., Tomas, A., Schoemaker, C., and Fittschen, C.: Rate constant of the reaction between CH₃O₂
553 and OH radicals revisited, J. Phys. Chem. A, 120, 8923-8932, 2016
554
555 Assaf, E., Sheps, L., Whalley, L., Heard, D., Tomas, A., Schoemaeker, C., and Fittschen, C.: The reaction
556 between CH₃O₂ and OH radicals: Product yields and atmospheric implications, Environ. Sci. Technol., 51, 4,
557 2170-2177, doi: 10.1021/acs.est.6b06265, 2017
558
559 Atkinson, R., Baulch, D.L., Cox, R.A., Crowley, J.N., Hampson, R.F., Hynes, R.G., Jenkin, M.E., Rossi, M. J.,
560 and Troe, J.: Evaluated kinetic and photochemical data for atmospheric chemistry: Volume III – gas phase
561 reactions of inorganic halogens, Atmos. Chem. Phys., 7, 981–1191, doi:10.5194/acp-7-981-2007, 2007
562
563 Barkley, M.P., Palmer, P.I., Ganzeveld, L., Arneth, A., Hagberg, D., Karl, T., Guenther, A., Paulot, F., Wennberg,
564 P.O., Mao, J.Q., Kurosu, T.P., Chance, K., Muller, J.-F., De Smedt, I., van Roozendaal, M., Chen, D., Wang,
565 Y.X., and Yantosca, R.M.: Can a “state of the art” chemistry transport model simulate Amazonian tropospheric
566 chemistry? J. Geophys. Res. Atmos., 116, D16302, 1-28, doi:10.1029/2011JD015893, 2011
567
568 Bell, N., Hsu, L., Jacob, D.J., Schultz, M.G., Blake, D.R., Butler, J.H., King, D.B., Lobert, J.M., and Maier-
569 Reimer, E.: Methyl iodide: Atmospheric budget and use as a tracer of marine convection in global models, J.
570 Geophys. Res. Atmos., 107, ACH 8-1–ACH 8-12, doi:10.1029/2001jd001151, 2002
571
572 Bey, I., Jacob, D.J., Yantosca, R.M., Logan, J.A., Field, B.D., Fiore, A.M., Li, Q., Liu, H.Y., Mickley, L.J.,
573 Schultz, M.G.: Global modelling of tropospheric chemistry with assimilated meteorology: Model description and
574 evaluation, J. Geophys. Res., 106, D19, 23073-23095, 2001
575
576 Bian, H.S., and Prather, M.J.: Fast-J2: Accurate simulation of stratospheric photolysis in global chemistry models,
577 J. Atmos. Chem., 41, 3, 281-296, 2002
578
579 Bitter, M., Ball, S., Povey, I., and Jones, R.: A broadband cavity ringdown spectrometer for in-situ measurements
580 of atmospheric trace gases, Atmos. Chem. Phys., 5, 3491–3532, doi:10.5194/acp-5-3491-2005, 2005
581
582 Bloss, W.J., Lee, J.D., Johnson, G.P., Sommariva, R., Heard, D.E., Saiz-Lopez, A., Plane, J.M.C., McFiggans,
583 G., Coe, H., Flynn, M., Williams, P., Rickard, A.R., Fleming, Z.: Impact of halogen monoxide chemistry upon
584 boundary layer OH and HO₂ concentrations at a coastal site, Geophys. Res. Lett., 32, L06814,
585 doi:10.1029/2004GL022084, 2005a
586



- 587 Bloss, W.J., Evans, M.J., Lee, J.D., Sommariva, R., Heard, D.E., Pilling, M.J.: The oxidative capacity of the
588 troposphere: Coupling of field measurements of OH and a global chemistry transport model, *Faraday. Discuss.*,
589 130, 425-436, 2005b
590
- 591 Bloss, W.J., Lee, J.D., Heard, D.E., Salmon, Bauguitte, S.J.-B., Roscoe, H.K., Jones, A.E.: Observations of OH
592 and HO₂ radicals in coastal Antarctica, *Atmos. Chem. Phys.*, 7, 4171-4185, 2007
593
- 594 Bloss, W.J., Camredon, M., Lee, J.D., Heard, D.E., Plane, J.M.C., Saiz-Lopez, A., Bauguitte, S.J.-B., Salmon,
595 R.A., Jones, A.E.: Coupling of HO_x, NO_x and halogen chemistry in the Antarctic boundary layer, *Atmos. Chem.*
596 *Phys.*, 10, 10187-10290, 2010
597
- 598 Bossolasco, A., Farago, E.P., Schoemaker, C., and Fittschen, C.: Rate constant of the reaction between CH₃O₂
599 and OH radicals, *Chem. Phys. Lett.*, 593, 7-13, 2014
600
- 601 Carpenter, L. J., Fleming, Z. L., Read, K. A., Lee, J. D., Moller, S.J., Hopkins, J., Purvis, R., Lewis, A. C., Muller,
602 K., Heinold, B., Herrmann, H., Wadinga Fomba, K., van Pinxteren, D., Muller, C., Tegen, I., Wiedensohler, A.,
603 Muller, T., Niedermeier, N., Achterberg, E. P., Patey, M. D., Kozlova, E. A., Heimann, M., Heard, D. E., Plane,
604 J. M. C., Mahajan, A., Oetjen, H., Ingham, T., Stone, D., Whalley, L., Evans, M., Pilling, M. J., Leigh, R. J.,
605 Monks, P. S., Karunaharan, A., Vaughan, S., Tschirner, J., Pohler, D., Frieß, U., Holla, R., Mendes, L., Lopez,
606 H., Faria, B., Manning, A. J., and Wallace, D. W. R.: Seasonal characteristics of tropical marine boundary layer
607 air measured at the Cape Verde Atmospheric Observatory, *J. Atmos. Chem.*, 67, 87–140, 2010
608
- 609 Carpenter, L.J., MacDonald, S.M., Shaw, M.D., Kumar, R., Saunders, R.W., Parthipan, R., Wilson, J., and Plane,
610 J.M.C.: Atmospheric iodine levels influenced by sea surface emissions of inorganic iodine, *Nat. Geosci.*, 6, 108–
611 111, doi:10.1038/ngeo1687, 2013
612
- 613 Carslaw, N., Creasey, D. J., Heard, D. E., Lewis, A. C., McQuaid, J. B., Pilling, M. J., Monks, P. S., Bandy, B. J.,
614 and Penkett, S. A.: Modeling OH, HO₂, and RO₂ radicals in the marine boundary layer – 1. Model construction
615 and comparison with field measurements, *J. Geophys. Res.*, 104(D23), 30 241–30 255, 1999
616
- 617 Carslaw, N., Creasey, D. J., Heard, D. E., Jacobs, P. J., Lee, J. D., Lewis, A. C., McQuaid, J. B., Pilling, M. J.,
618 Bauguitte, S., Penkett, S. A., Monks, P. S., Salisbury, G.: Eastern Atlantic Spring Experiment 1997 (EASE97) –
619 2. Comparisons of model concentrations of OH, HO₂, and RO₂ with measurements, *J. Geophys. Res.-Atmos.*,
620 107(D14), 4190, 2002
621
- 622 Commane, R., Seitz, K., Bale, C.S.E., Bloss, W.J., Buxmann, J., Ingham, T., Platt, U., Pohler, D., Heard, D.E.:
623 Iodine monoxide at a clean marine coastal site: observations of high frequency variations and inhomogeneous
624 distributions, *Atmos. Chem. Phys.*, 11, 6721-6733, 2011
625
- 626 Dix, B., Baidar, S., Bresch, J.F., Hall, S.R., Schmidt, S., Wang, S., Volkamer, R.: Detection of iodine monoxide
627 in the tropical free troposphere, *Proc. Nat. Acad. Sci.*, 110, 6, 2035-2040
628



- 629 Edwards, P., Evans, M.J., Commane, R., Ingham, T., Stone, D., Mahajan, A.S., Oetjen, H., Dorsey, J.R., Hopkins,
630 J.R., Lee, J.D., Moller, S.J., Leigh, R., Plane, J.M.C., Carpenter, L.J., Heard, D.E.: Hydrogen oxide
631 photochemistry in the northern Canadian spring time boundary layer, *J. Geophys. Res.*, 116, D22306.
632 Doi:10.1029/2011JD016390, 2011
633
- 634 Ehhalt, D.H., Rohrer, F.: The tropospheric cycle of H₂: a critical review, *Tellus*, 61B, 500-535, 2009
635
- 636 Emmerson, K.M., Evans, M.J.: Comparison of tropospheric gas-phase chemistry schemes for use within global
637 models, *Atmos. Chem. Phys.*, 9, 1831-1845, 2009
638
- 639 Evans, M. J., Jacob, D. J.: Impact of new laboratory studies of N₂O₅ hydrolysis on global model budgets of
640 tropospheric nitrogen oxides, ozone, and OH, *Geophys. Res. Lett.*, 32, 1–4, 2005
641
- 642 Fairlie, T.D., Jacob, D.J., and Park, R.J.: The impact of transpacific transport of mineral dust in the United States,
643 *Atmos. Environ.*, 41, 6, 1251-1266, doi:10.1016/j.atmosenv.2006.09.048, 2007
644
- 645 Fischer, E.V., Jacob, D.J., Millet, D.B., Yantosca, R.M., and Mao, J.: The role of the ocean in the global
646 atmospheric budget of acetone, *Geophys. Res. Lett.*, 39, L01807, doi:10.1029/2011gl050086, 2012
647
- 648 Fittschen, C., Whalley, L.K., and Heard, D.E.: The reaction of CH₃O₂ radicals with OH radicals: A neglected sink
649 for CH₃O₂ in the remote atmosphere, *Environ. Sci. Technol.*, 118, 7700-7701, 2014
650
- 651 Fomba, K.W., Muller, K., van Pinxteren, D., Poulain, L., van Pinxteren, M., and Herrmann, H., Long-term
652 chemical characterization of tropical and marine aerosols at the Cape Verde Atmospheric Observatory (CVAO)
653 from 2007 to 2011, *Atmos. Chem. Phys.*, 14, 17, 8883-8904, doi:10.5194/acp-14-8883-2014, 2014
654
- 655 Fu, T.-M., Jacob, D.J., Wittrock, F., Burrows, J.P., Vrekoussis, M., and Henze, D.K.: Global budgets of
656 atmospheric glyoxal and methylglyoxal, and implications for formation of secondary organic aerosols, *J.*
657 *Geophys. Res.*, 113, D15303, doi:10.1029/2007jd009505, 2008
658
- 659 Fuchs, H., Bohn, B., Hofzumahaus, A., Holland, F., Lu, K. D., Nehr, S., Rohrer, F., Wahner, A.: Detection of
660 HO₂ by laser induced fluorescence: calibration and interferences from RO₂ radicals, *Atmos. Meas. Tech.*, 4, 1209–
661 1225, 2011
662
- 663 George, I.J., Matthews, P.S.J., Whalley, L.K., Brooks, B., Goddard, A., Baeza-Romero, M.T., Heard, D.E.:
664 Measurements of uptake coefficients for heterogeneous loss of HO₂ onto submicron inorganic salt aerosols, *Phys.*
665 *Chem. Chem. Phys.*, 15, 12829-12845, 2013
666
- 667 Gomez Martin, J.C., Mahajan, A.S., Hay, T.D., Prados-Roman, C., Ordonez, C., MacDonald, S.M., Plane, J.M.C.,
668 Sorribas, M., Gil, M., Francisco Paredes Mora, J., Agama Reyes, M.V., Oram, D.E., Leedham, E., Saiz-Lopez,
669 A.: Iodine chemistry in the eastern Pacific marine boundary layer, *J. Geophys. Res. Atmos.*, 118, 887-904, 2013
670



- 671 Guenther, A., Karl, T., Harley, P., Wiedinmyer, C., Palmer, P.I., and Geron, C.: Estimates of global terrestrial
672 isoprene emissions using MEGAN (Model of Emissions of Gases and Aerosols from Nature), Atmos. Chem.
673 Phys., 6, 3181-3210, 2006
674
- 675 Heald, C.L., Coe, H., Jimenez, J.L., Weber, R.J., Bahreini, R., Middlebrook, A.M., Russell, L.M., Jolleys, M.,
676 Fu, T.M., Allan, J.D., Bower, K.N., Capes, G., Crosier, J., Morgan, W.T., Robinson, N.H., Williams, P.I.,
677 Cubison, M.J., De Carlo, P.F., and Dunlea, E.J.: Exploring the vertical profile of atmospheric organic aerosol:
678 comparing 17 aircraft field campaigns with a global model, Atmos. Chem. Phys., 11, 24, 12673-12696,
679 doi:10.5194/acp-11-12673-2011, 2011
680
- 681 Heard, D. E., Read, K. A., Methven, J., Al-Haider, S., Bloss, W. J., Johnson, G. P., Pilling, M. J., Seakins, P. W.,
682 Smith, S. C., Sommariva, R., Stanton, J. C., Still, T. J., Ingham, T., Brooks, B., De Leeuw, G., Jackson, A. V.,
683 McQuaid, J. B., Morgan, R., Smith, M. H., Carpenter, L. J., Carslaw, N., Hamilton, J., Hopkins, J. R., Lee, J. D.,
684 Lewis, A. C., Purvis, R. M., Wevill, D. J., Brough, N., Green, T., Mills, G., Penkett, S. A., Plane, J. M. C., Saiz-
685 Lopez, A., Worton, D., Monks, P. S., Fleming, Z., Rickard, A. R., Alfarra, M. R., Allan, J. D., Bower, K., Coe,
686 H., Cubison, M., Flynn, M., McFiggans, G., Gallagher, M., Norton, E. G., O'Dowd, C. D., Shillito, J., Topping,
687 D., Vaughan, G., Williams, P., Bitter, M., Ball, S. M., Jones, R. L., Povey, I. M., O'Doherty, S., Simmonds, P.
688 G., Allen, A., Kinnersley, R. P., Beddows, D. C. S., Dall'Osto, M., Harrison, R. M., Donovan, R. J., Heal, M. R.,
689 Jennings, S. G., Noone, C., Spain, G.: The North Atlantic Marine Boundary Layer Experiment (NAMBLEX).
690 Overview of the campaign held at Mace Head, Ireland, in summer 2002, Atmos. Chem. Phys., 6, 2241–2272,
691 doi:10.5194/acp-6-2241-2006, 2006
692
- 693 Henze, D.K., Hakami, A., and Seinfeld, J.H.: Development of the adjoint of GEOS-Chem, Atmos. Chem. Phys.,
694 7, 9, 2413-2433, 2007
695
- 696 Henze, D.K., Seinfeld, J.H., and Shindell, D.T.: Inverse modeling and mapping US air quality influences of
697 inorganic PM_{2.5} precursor emissions using the adjoint of GEOS-Chem, Atmos. Chem. Phys., 9, 16, 5877-5903,
698 2009
699
- 700 Hoffmann, T., O'Dowd, C.D., and Seinfeld, J.H.: Iodine oxide homogeneous nucleation: An explanation for
701 coastal new particle production, Geophys. Res. Lett., 28, 10, 1949-1952, doi:10.1029/2000GL012399, 2001
702
- 703 Holmes, C.D., Jacob, D.J., and Yang, X.: Global lifetime of elemental mercury against oxidation by atomic
704 bromine in the free troposphere, Geophys. Res. Lett., 33, L20808, doi:10.1029/2006gl027176, 2006
705
- 706 Holmes, C.D., Jacob, D.J., Corbitt, E.S., Mao, J., Yang, X., Talbot, R., and Slemr, F.: Global atmospheric model
707 for mercury including oxidation by bromine atoms, Atmos. Chem. Phys., 10, 12037–12057, doi:10.5194/acp-10-
708 12037-2010, 2010
709
- 710 Hu, L., Jacob, D.J., Liu, X., Zhang, Y., Zhang, L., Kim, P.S., Sulprizio, M.P., and Yantosca, R.M.: Global budget
711 of tropospheric ozone: Evaluating recent model advances with satellite (OMI), aircraft (IAGOS), and ozonesonde
712 observations, Atmos. Environ., doi:10.1016/j.atmosenv.2017.08.036, 2017
713



- 714 Jacob, D.J.: Heterogeneous chemistry and tropospheric ozone, *Atmos. Environ.*, 34, 2131–2159,
715 doi:10.1016/S1352-2310(99)00462-8, 2000
716
- 717 Jacobson, M.Z. and Turco, R.P.: SMVGEAR: A sparse-matrix, vectorized gear code for atmospheric models,
718 *Atmos. Environ.*, 28, 273–284, 1994
719
- 720 Jaeglé, L., Quinn, P.K., Bates, T.S., Alexander, B., and Lin, J.-T.: Global distribution of sea salt aerosols: new
721 constraints from in situ and remote sensing observations, *Atmos. Chem. Phys.*, 11, 3137–3157, doi:10.5194/acp-
722 11-3137-2011, 2011
723
- 724 Jenkin, M.E., Saunders, S.M., Wagner, V., Pilling, M.J., Protocol for the development of the Master Chemical
725 Mechanism, MCM v3 (Part B): tropospheric degradation of aromatic volatile organic compounds, *Atmos. Chem.*
726 *Phys.*, 3, 181–193, 2003
727
- 728 Kanaya, Y., Matsumoto, J., Kato, S., and Akimoto, H.: Behavior of OH and HO₂ radicals during the Observations
729 at a Remote Island of Okinawa (ORION99) field campaign. 2. Comparison between observations and
730 calculations, *J. Geophys. Res.-Atmos.*, 106, 24209–24223, 2001
731
- 732 Kanaya, Y., Yokouchi, Y., Matsumoto, J., Nakamura, K., Kato, S., Tanimoto, H., Furutani, H., Toyota, K., and
733 Akimoto, H.: Implications of iodine chemistry for daytime HO₂ levels at Rishiri Island, *Geophys. Res. Lett.*, 29,
734 1212, doi:10.1029/2001GL014061, 2002
735
- 736 Kanaya, Y., Cao, R., Kato, S., Miyakawa, Y., Kajii, Y., Tanimoto, H., Yokouchi, Y., Mochida, M., Kawamura,
737 K., Akimoto, H.: Chemistry of OH and HO₂ radicals observed at Rishiri Island, Japan, in September 2003:
738 Missing daytime sink of HO₂ and positive nighttime correlations with monoterpenes, *J. Geophys. Res.-Atmos.*,
739 112, D11308, doi:10.1029/2006JD007987, 2007
740
- 741 Lakey, P.S.J., George, I.J., Whalley, L.K., Baeza-Romero, M.T., and Heard, D.E.: Measurements of HO₂ uptake
742 coefficients onto single component organic aerosols, *Environ. Sci. Technol.*, 49, 8, 4878–4885,
743 doi:10.1021/acs.est.5b00948, 2015
744
- 745 Lee, J.D., Moller, S.J., Read, K.A., Lewis, A.C., Mendes, L., Carpenter, L.J.: Year-round measurements of
746 nitrogen oxides and ozone in the tropical North Atlantic marine boundary layer, *J. Geophys. Res.*, 114, D21302,
747 doi:10.1029/2009JD011878, 2009
748
- 749 Lee, J. D., McFiggans, G., Allan, J. D., Baker, A. R., Ball, S. M., Benton, A. K., Carpenter, L. J., Commane, R.,
750 Finley, B. D., Evans, M., Fuentes, E., Furneaux, K., Goddard, A., Good, N., Hamilton, J. F., Heard, D. E.,
751 Herrmann, H., Hollingsworth, A., Hopkins, J. R., Ingham, T., Irwin, M., Jones, C. E., Jones, R. L., Keene, W. C.,
752 Lawler, M. J., Lehmann, S., Lewis, A. C., Long, M. S., Mahajan, A., Methven, J., Moller, S. J., Miller, K., Muller,
753 T., Niedermeier, N., O'Doherty, S., Oetjen, H., Plane, J. M. C., Pszenny, A. A. P., Read, K. A., Saiz-Lopez, A.,
754 Saltzman, E. S., Sander, R., von Glasow, R., Whalley, L., Wiedensohler, A., Young, D.: Reactive Halogens in
755 the Marine Boundary Layer (RHAMBLe): the tropical North Atlantic experiments, *Atmos. Chem. Phys.*, 10,
756 1031–1055, 2010



- 757
758 Leser, H., Honninger, G., Platt, U.: MAX-DOAS measurements of BrO and NO₂ in the marine boundary layer,
759 Geophys. Res. Lett., 30, doi:10.1029/2002GL015 811, 2003
760
- 761 Liao, H., Henze, D.K., Seinfeld, J.H., Wu, S.L., and Mickley, L.J.: Biogenic secondary organic aerosol over the
762 United States: Comparison of climatological simulations with observations, J. Geophys. Res. Atmos., 112, D6,
763 D06201, 1-19, doi:10.1029/2006JD007813, 2007
764
- 765 Liu, H., Jacob, D.J., Bey, I., and Yantosca, R.M.: Constraints from ²¹⁰Pb and ⁷Be on wet deposition and transport
766 in a global three-dimensional chemical tracer model driven by assimilated meteorological fields, J. Geophys.
767 Res., 106, 12109–12128, doi:10.1029/2000jd900839, 2001
768
- 769 MacDonald, S.M., Gómez Martín, J.C., Chance, R., Warriner, S., Saiz-Lopez, A., Carpenter, L.J., and Plane,
770 J.M.C.: A laboratory characterisation of inorganic iodine emissions from the sea surface: dependence on oceanic
771 variables and parameterisation for global modelling, Atmos. Chem. Phys., 14, 5841–5852, doi:10.5194/acp-14-
772 5841-2014, 2014
773
- 774 Mahajan, A.S., Plane, J.M.C., Oetjen, H., Mendes, L., Saunders, R.W., Saiz-Lopez, A., Jones, C.E., Carpenter,
775 L.J., McFiggans, G.B.: Measurement and modelling of tropospheric reactive halogen species over the tropical
776 Atlantic Ocean, Atmos. Chem. Phys., 10, 4611-4624, 2010a
777
- 778 Mahajan, A.S., Whalley, L.K., Kozlova, E., Oetjen, H., Mendez, L., Furneaux, K.L., Goddard, A., Heard, D.E.,
779 Plane, J.M.C., Saiz-Lopez, A.: DOAS observations of formaldehyde and its impact on the HO_x balance in the
780 tropical Atlantic marine boundary layer, J. Atmos. Chem., 66, 167-178, 2010b
781
- 782 Mahajan, A. S., Sorribas, M., Gomez Martn, J. C., MacDonald, S. M., Gil, M., Plane, J. M. C., Saiz-Lopez, A.:
783 Concurrent observations of atomic iodine, molecular iodine and ultrafine particles in a coastal environment,
784 Atmos. Chem. Phys., 11, 2545–2555, doi:10.5194/acp-11-2545-2011, 2011
785
- 786 Mao, J., Jacob, D.J., Evans, M.J., Olson, J.R., Ren, X., Brune, W.H., Clair, J.M. St., Crouse, J.D., Spencer, K.M.,
787 Beaver, M.R., Wennberg, P.O., Cubison, M.J., Jimenez, J.L., Fried, A., Weibring, P., Walega, J.G., Hall, S.R.,
788 Weinheimer, A.J., Cohen, R.C., Chen, G., Crawford, J.H., McNaughton, C., Clarke, A.D., Jaegle, L., Fisher, J.A.,
789 Yantosca, R.M., Le Sager, P., and Carouge, C.: Chemistry of hydrogen oxide radicals (HO_x) in the Arctic
790 troposphere in spring, Atmos. Chem. Phys., 10, 5823–5838, doi:10.5194/acp-10-5823-2010, 2010
791
- 792 Mao, J., Fan, S., Jacob, D.J., Travis, K.R.: Radical loss in the atmosphere from Cu-Fe redox coupling in aerosols,
793 Atmos. Chem. Phys., 13, 509-519, 2013
794
- 795 Matthews, P.S.J., Baeza-Romero, M.T., Whalley, L.K., and Heard, D.E.: Uptake of HO₂ radicals onto Arizona
796 test dust particles using an aerosol flow tube, Atmos. Chem. Phys., 14, 7397-7408, doi:10.5194/acp-14-7397-
797 2014, 2014
798



- 799 McFiggans, G., Coe, H., Burgess, R., Allan, J., Cubison, M., Alfarra, M. R., Saunders, R., Saiz-Lopez, A., Plane,
800 J. M. C., Wevill, D., Carpenter, L., Rickard, A. R., Monks, P. S.: Direct evidence for coastal iodine particles from
801 *Laminaria* macroalgae – linkage to emissions of molecular iodine, Atmos. Chem. Phys., 4, 701–713,
802 doi:10.5194/acp-4-701-2004, 2004
803
- 804 McFiggans, G., Bale, C. S. E., Ball, S. M., Beames, J. M., Bloss, W.J., Carpenter, L. J., Dorsey, J., Dunk, R.,
805 Flynn, M. J., Furneaux, K. L., Gallagher, M. W., Heard, D. E., Hollingsworth, A. M., Hornsby, K., Ingham, T.,
806 Jones, C. E., Jones, R. L., Kramer, L. J., Langridge, J. M., Leblanc, C., LeCrane, J.-P., Lee, J. D., Leigh, R. J.,
807 Longley, I., Mahajan, A. S., Monks, P. S., Oetjen, H., Orr-Ewing, A. J., Plane, J. M. C., Potin, P., Shillings, A. J.
808 L., Thomas, F., von Glasow, R., Wada, R., Whalley, L. K., Whitehead, J. D.: Iodine-mediated coastal particle
809 formation: an overview of the Reactive Halogens in the Marine Boundary Layer (RHAMBLe) Roscoff coastal
810 study, Atmos. Chem. Phys., 10, 2975–2999, doi:10.5194/acp-10-2975-2010, 2010
811
- 812 McLinden, C.A., Olsen, S.C., Hannegan, B., Wild, O., Prather, M.J., and Sundet, J.: Stratospheric ozone in 3-D
813 models: A simple chemistry and the cross-tropopause flux, J. Geophys. Res., 105, 14653–14665, 2000
814
- 815 Millet, D.B., Bassandorj, M., Farmer, D.K., Thornton, J.A., Baumann, K., Brophy, P., Chaliyakunnel, S., de
816 Gouw, J.A., Graus, M., Hu, L., Koss, A., Lee, B.H., Lopez-Hilfiker, F.D., Neuman, J.A., Paulot, F., Peischl, J.,
817 Pollack, I.B., Ryerson, T.B., Warneke, C., Williams, B.J., and Xu, J.: A large and ubiquitous source of
818 atmospheric formic acid, Atmos. Chem. Phys., 15, 6283–6304, doi:10.5194/acp-15-6283-2015, 2015
819
- 820 Muller, K., Lehmann, S., van Pinxteren, D., Gnauk, T., Niedermeier, N., Wiedensohler, A., Herrmann, H.: Particle
821 characterization at the Cape Verde atmospheric observatory during the 2007 RHAMBLe intensive, Atmos. Chem.
822 Phys., 10, 2709–2721, 2010
823
- 824 Murray, L.T., Jacob, D.J., Logan, J.A., Hudman, R.C., and Koshak, W.J.: Optimized regional and interannual
825 variability of lightning in a global chemical transport model constrained by LIS/OTD satellite data, J. Geophys.
826 Res. Atmos., 117, D20307, doi:10.1029/2012JD017934, 2012
827
- 828 Nassar, R., Logan, J. A., Megretskaia, I. A., Murray, L. T., Zhang, L., and Jones, D. B. A.: Analysis of tropical
829 tropospheric ozone, carbon monoxide, and water vapour during the 2006 El Nino using TES observations and the
830 GEOS-Chem model, J. Geophys. Res., 114, D17304, doi:10.1029/2009JD011760, 2009
831
- 832 NOAA CMDL flask analysis, <ftp://ftp.cmdl.noaa.gov/ccg/ch4/>, GLOBALVIEW-CH4, 2010–2011: Cooperative
833 Atmospheric Data Integration Project – Methane. CD-ROM, NOAA ESRL, Boulder, Colorado, also available on
834 Internet via anonymous FTP to <ftp://ftp.cmdl.noaa.gov/ccg/ch4/>, path: ccg/CH4/GLOBALVIEW, 2009, access:
835 17 Feb 2010
836
- 837 Novelli, P.C., Lang, P.M., Masarie, K.A., Hurst, D.F., Myers, R., Elkins, J.W.: Molecular hydrogen in the
838 troposphere: Global distribution and budget, J. Geophys. Res., 104, D23, 30,427–30,444, 1999
839
- 840 O’Dowd, C.D. and Hoffmann, T.: Coastal new particle formation: a review of the current state-of-the-art, Environ.
841 Chem., 2, 245, doi:10.1071/EN05077, 2005



- 842
843 Olivier, J.G.J., and Peters, J.A.H.W.: CO₂ from non-energy use of fuels: A global, regional and national
844 perspective based on the IPCC Tier 1 approach, *Res. Conserv., Recycl.*, 45, 3, 210-225,
845 doi:10.1016/j.resconrec.2005.05.008, 2005
846
- 847 Ordonez, C., Lamarque, J.-F., Tilmes, S., Kinnison, D.E., Atlas, E.L., Blake, D.R., Sousa Santos, G., Brasseur,
848 G., Saiz-Lopez, A.: Bromine and iodine chemistry in a global chemistry-climate model: description and
849 evaluation of very short-lived oceanic sources, *Atmos. Chem. Phys.*, 12, 1423-1447, 2012
850
- 851 Park, R.J., Jacob, D.J., Field, B.D., Yantosca, R.M., and Chin, M.: Natural and transboundary pollution influences
852 on sulfate-nitrate-ammonium aerosols in the United States: Implications for policy, *J. Geophys. Res. Atmos.*, 109,
853 D15204, doi:10.1029/2003JD004473, 2004
854
- 855 Parrella, J.P., Jacob, D.J., Liang, Q., Zhang, Y., Mickley, L.J., Miller, B., Evans, M.J., Yang, X., Pyle, J.A., Theys,
856 N., Van Roozendael, M.: Tropospheric bromine chemistry: implications for present and pre-industrial ozone and
857 mercury, *Atmos. Chem. Phys.*, 12, 6723-6740, 2012
858
- 859 Paulot, F., Crouse, J.D., Kjaergaard, H.G., K^uurten, A., St. Clair, J.M., Seinfeld, J.H., and Wennberg, P.O.:
860 Unexpected Epoxide Formation in the Gas-Phase Photooxidation of Isoprene, *Science*, 325, 730–733, 2009
861
- 862 Peters, C., Pechtl, S., Stutz, J., Hebestreit, K., Honninger, G., Heumann, K. G., Schwarz, A., Winterlik, J., and
863 Platt, U.: Reactive and organic halogen species in three different European coastal environments, *Atmos. Chem.*
864 *Phys.*, 5, 3357–3375, doi:10.5194/acp-5-3357-2005, 2005
865
- 866 Pye, H.O.T., Liao, H., Wu, S., Mickley, L.J., Jacob, D.J., Henze, D.K., and Seinfeld, J.H.: Effect of changes in
867 climate and emissions on future sulfate-nitrate-ammonium aerosol levels in the United States, *J. Geophys. Res.*
868 *Atmos.*, 114, D01205, doi:10.1029/2008JD010701, 2009
869
- 870 Read, K. A., Mahajan, A. S., Carpenter, L. J., Evans, M. J., Faria, B. V. E., Heard, D. E., Hopkins, J. R., Lee, J.
871 D., Moller, S. J., Lewis, A. C., Mendes, L., McQuaid, J. B., Oetjen, H., Saiz-Lopez, A., Pilling, M. J., Plane, J.
872 M. C.: Extensive halogen mediated ozone destruction over the tropical Atlantic Ocean, *Nature*, 453, 7199, 1232–
873 1235, 2008
874
- 875 Saiz-Lopez, A. and Plane, J. M. C.: Novel iodine chemistry in the marine boundary layer, *Geophys. Res. Lett.*,
876 31, L04112, doi:10.1029/2003GL019215, 2004
877
- 878 Saiz-Lopez, A., Plane, J. M. C., Shillito, J. A.: Bromine oxide in the mid-latitude marine boundary layer, *Geophys.*
879 *Res. Lett.*, 31, L03111, doi:10.1029/2003GL018956, 2004
880
- 881 Saiz-Lopez, A., Shillito, J.A., Coe, H., Plane, J.M.C.: Measurements and modelling of I₂, IO, OIO, BrO and NO₃
882 in the mid-latitude marine boundary layer, *Atmos. Chem. Phys.*, 6, 1513-1528, 2006
883



- 884 Saiz-Lopez, A., Lamarque, J.-F., Kinnison, D.E., Tilmes, S., Ordonez, C., Orlando, J.J., Conley, A.J., Plane,
885 J.M.C., Mahajan, A.S., Sousa Santos, G., Atlas, E.L., Blake, D.R., Sander, S.P., Schauffler, S., Thompson, A.M.,
886 Brasseur, G.: Estimating the climate significance of halogen-driven ozone loss in the tropical marine troposphere,
887 Atmos. Chem. Phys., 12, 3939-3949, 2012
888
- 889 Saiz-Lopez, A., von Glasow, R.: Reactive halogen chemistry in the troposphere, Chem. Soc. Rev., 41, 6448-6472,
890 2012
891
- 892 Sander, R., Keene, W. C., Pszenny, A. A. P., Arimoto, R., Ayers, G. P., Baboukas, E., Caine, J. M., Crutzen, P.
893 J., Duce, R. A., Honninger, G., Huebert, B. J., Maenhaut, W., Mihalopoulos, N., Turekian, V. C., Van Dingenen,
894 R.: Inorganic bromine in the marine boundary layer: a critical review, Atmos. Chem. Phys., 3, 1301-1336,
895 doi:10.5194/acp-3-1301-2003, 2003
896
- 897 Sander, S.P., Friedl, R.R., Abbatt, J.P.D., Barker, J.R., Burkholder, J.B., Golden, D.M., Kolb, C.E., Kurylo, M.J.,
898 Moortgat, G.K., Wine, P., Huie, R.E., and Orkin, V.L.: Chemical kinetics and photochemical data for use in
899 atmospheric studies, Evaluation Number 17, Tech. rep., NASA Jet Propulsion Laboratory, Pasadena, 2011
900
- 901 Sandu, A., Sander, R.: Technical note: Simulating chemical systems in Fortran90 and Matlab with the Kinetic
902 PreProcessor KPP-2.1, Atmos. Chem. Phys., 6, 187-195, 2006
903
- 904 Saunders, S.M., Jenkin, M.E., Derwent, R.G., Pilling, M.J.: Protocol for the development of the Master Chemical
905 Mechanism, MCM v3 (Part A): tropospheric degradation of non-aromatic volatile organic compounds, Atmos.
906 Chem. Phys., 3, 161-180, 2003
907
- 908 Schmidt, J.A., Jacob, D.J., Horowitz, H.M., Hu, L., Sherwen, T., Evans, M.J., Liang, Q., Suleiman, R.M., Oram,
909 D.E., Breton, M.L., Percival, C.J., Wang, S., Dix, B., and Volkamer, R.: Modeling the observed tropospheric BrO
910 background: Importance of multiphase chemistry and implications for ozone, OH, and mercury, J. Geophys. Res.
911 Atmos., 121, 19, 11819-11835, doi:10.1002/2015JD024229, 2016
912
- 913 Schwarz, S. E.: Mass-transport considerations pertinent to aqueous phase reactions of gases in liquid-water
914 clouds, Chemistry of Multiphase Atmospheric Systems, NATO ASI Series, G6, Jaeschke ed., Springer-Verlag,
915 Berlin, 415-471, 1986
916
- 917 Sherwen, T., Evans, M.J., Carpenter, L.J., Andrews, S.J., Lidster, R.T., Dix, B., Koenig, T.K., Sinreich, R.,
918 Ortega, I., Volkamer, R., Saiz-Lopez, A., Prados-Roman, C., Mahajan, A. S., and Ordóñez, C.: Iodine's impact
919 on tropospheric oxidants: a global model study in GEOS-Chem, Atmos. Chem. Phys., 16, 1161-1186,
920 doi:10.5194/acp-16-1161-2016, 2016a
921
- 922 Sherwen, T., Schmidt, J.A., Evans, M.J., Carpenter, L.J., Großmann, K., Eastham, S.D., Jacob, D.J., Dix, B.,
923 Koenig, T.K., Sinreich, R., Ortega, I., Volkamer, R., Saiz-Lopez, A., Prados-Roman, C., Mahajan, A.S., and
924 Ordóñez, C.: Global impacts of tropospheric halogens (Cl, Br, I) on oxidants and composition in GEOS-Chem,
925 Atmos. Chem. Phys., 16, 12239-12271, doi:10.5194/acp-16-12239-2016, 2016b
926



- 927 Sherwen, T.M., Evans, M.J., Spracklen, D.V., Carpenter, L.J., Chance, R., Baker, A.R., Schmidt, J.A., and
928 Breider, T.J.: Global modeling of tropospheric iodine aerosol, *Geophys. Res. Lett.*, 43, 18, 19912-10019,
929 doi:10.1029/2016GL070062, 2016c
930
- 931 Sherwen, T., Evans, M.J., Carpenter, L.J., Schmidt, J.A., and Mickley, L.J.: Halogen chemistry reduces
932 tropospheric O₃ radiative forcing, *Atmos. Chem. Phys.*, 17, 1557-1569, doi:10.5194/acp-17-1557-2017, 2017
933
- 934 Simpson, W.R., Brown, S.S., Saiz-Lopez, A., Thornton, J.A., and von Glasow, R.: Tropospheric Halogen
935 Chemistry: Sources, Cycling, and Impacts, *Chem. Rev.*, 115, 4035–4062, doi:10.1021/cr5006638, 2015
936
- 937 Smith, S. C., Lee, J. D., Bloss, W. J., Johnson, G. P., Ingham, T., Heard, D. E.: Concentrations of OH and HO₂
938 radicals during NAMBLEX: measurements and steady state analysis, *Atmos. Chem. Phys.*, 6, 1435–1453, 2006
939
- 940 Sommariva, R., Bloss, W.J., Brough, N., Carslaw, N., Flynn, M., Haggerstone, A.-L., Heard, D.E., Hopkins, J.R.,
941 Lee, J.D., Lewis, A.C., McFiggans, G., Monks, P.S., Penkett, S.A., Pilling, M.J., Plane, J.M.C., Read, K.A., Saiz-
942 Lopez, A., Rickard, A.R., Williams, P.I.: OH and HO₂ chemistry during NAMBLEX: role of oxygenates, halogen
943 oxides and heterogeneous uptake, *Atmos. Chem. Phys.*, 6, 1135-1153, 2006
944
- 945 Sommariva, R., Pilling, M.J., Bloss, W.J., Heard, D.E., Lee, J.D., Fleming, Z.L., Monks, P.S., Plane, J.M.C.,
946 Saiz-Lopez, A., Ball, S.M., Bitter, M., Jones, R.L., Brough, N., Penkett, S.A., Hopkins, J.R., Lewis, A.C., Read,
947 K.A.: Night-time radical chemistry during the NAMBLEX campaign, *Atmos. Chem. Phys.*, 7, 587-598, 2007
948
- 949 Stone, D., Evans, M.J., Commane, R., Ingham, T., Floquet, C.F.A., McQuaid, J.B., Brookes, D.M., Monks, P.S.,
950 Purvis, R., Hamilton, J.F., Hopkins, J., Lee, J., Lewis, A.C., Stewart, D., Murphy, J.G., Mills, G., Oram, D.,
951 Reeves, C.E., Heard, D.E. : HO_x observations over West Africa during AMMA: Impact of isoprene and NO_x,
952 *Atmos. Chem. Phys.*, 10, 9415-9429, 2010
953
- 954 Stone, D., Evans, M.J., Edwards, P.M., Commane, R., Ingham, T., Rickard, A.R., Brookes, D.M., Hopkins, J.,
955 Leigh, R.J., Lewis, A.C., Monks, A.C., Monks, P.S., Oram, D., Reeves, C.E., Stewart, D., Heard, D.E.: Isoprene
956 oxidation mechanisms: measurements and modelling of OH and HO₂ over a South-East Asian tropical rainforest
957 during the OP3 field campaign, *Atmos. Chem. Phys.*, 11, 6749-6771, 2011
958
- 959 Stone, D., Whalley, L.K., Heard, D.E.: Tropospheric OH and HO₂ radicals: Field measurements and model
960 comparisons, *Chem. Soc. Rev.*, 41, 6348-6404, 2012
961
- 962 Stone, D., Evans, M.J., Walker, H., Ingham, T., Vaughan, S., Ouyang, B., Kennedy, O.J., McLeod, M.W., Jones,
963 R.L., Hopkins, J., Punjabi, S., Lidster, R., Hamilton, J.F., Lee, J.D., Lewis, A.C., Carpenter, L.J., Forster, G.,
964 Oram, D.E., Reeves, C.E., Bauguitte, S., Morgan, W., Coe, H., Aruffo, E., Dari-Salisburgo, C., Giammaria, F.,
965 Di Carlo, P., and Heard, D.E.: Radical Chemistry at Night: Comparisons between observed and modeled HO_x,
966 NO₃ and N₂O₅ during the RONOCO project, *Atmos. Chem. Phys.*, 14, 1299-1321, 2014, doi:10.5194/acp-14-
967 1299-2014
968



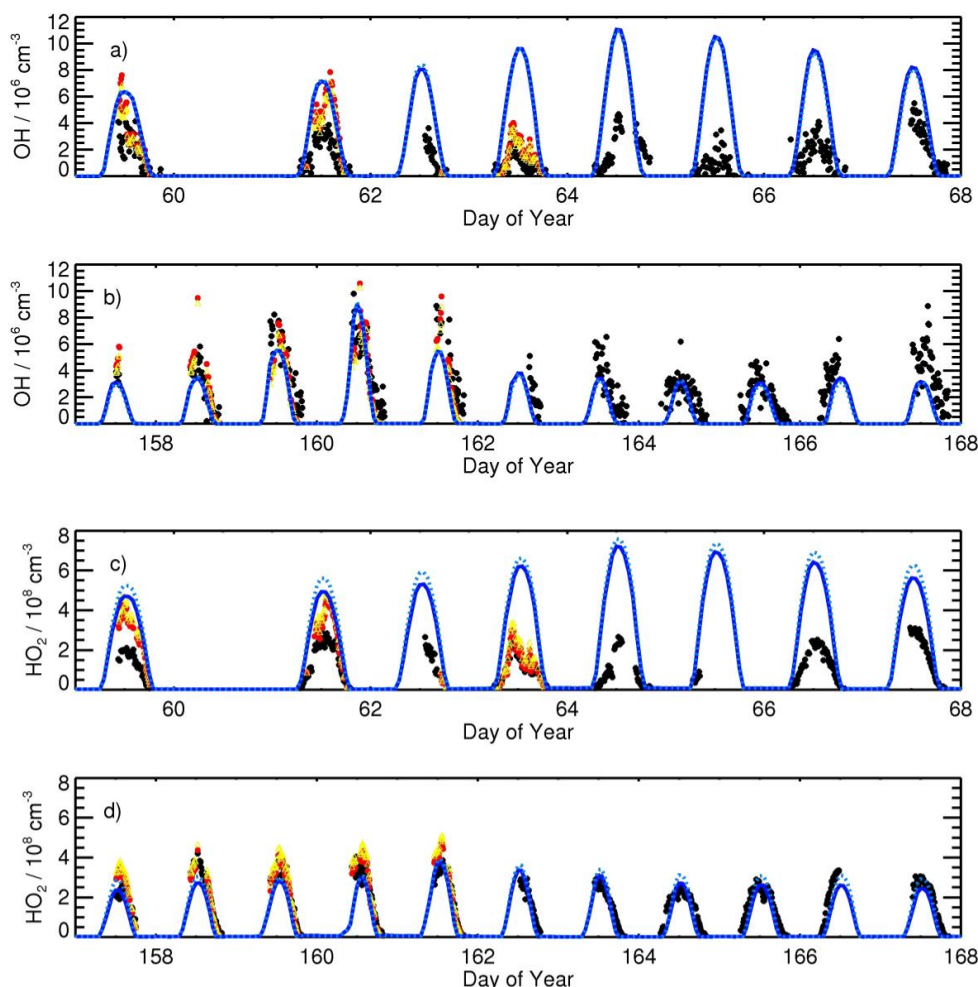
- 969 Taketani, F., Kanaya, Y., Akimoto, H.: Kinetics of heterogeneous reactions of HO₂ radical at ambient
970 concentration levels with (NH₄)₂SO₄ and NaCl aerosol particles, *J. Phys. Chem. A.*, 112, 11, 2370-2377, 2008
971
- 972 Theys, N., Van Roozendaal, M., Hendrick, F., Yang, X., De Smedt, I., Richter, A., Begoin, M., Errera, Q.,
973 Johnston, P.V., Kreher, K., and De Mazière, M.: Global observations of tropospheric BrO columns using GOME-
974 2 satellite data, *Atmos. Chem. Phys.*, 11, 1791–1811, doi:10.5194/acp-11-1791-2011, 2011
975
- 976 Thornton, J.A., Jaegle, L., and McNeill, V.F.: Assessing known pathways for HO₂ loss in aqueous atmospheric
977 aerosols: Regional and global impacts on tropospheric oxidants, *J. Geophys. Res. Atmos.*, 113, D5, D05303, 1-
978 16, doi:10.1029/2007JD009236, 2008
979
- 980 van het Bolscher, M., REanalysis of the TROspheric chemical composition over the past 40 years: A long-term
981 global modeling study of tropospheric chemistry funded under the 5th EU framework programme, *Rep. EU-*
982 *Contract No. EVK2-CT-2002-00170*, 1-77, MPI for Meteorology, Hamburg, Germany
983
- 984 Vaughan, S., Ingham, T., Whalley, L.K., Stone, D., Evans, M.J., Read, K.A., Lee, J.D., Moller, S.J., Carpenter,
985 L.J., Lewis, A.C., Fleming, Z.L., Heard, D.E.: Seasonal observations of OH and HO₂ in the remote tropical marine
986 boundary layer, *Atmos. Chem. Phys.*, 12, 2149-2172, 2012
987
- 988 Vogt, R., Crutzen, P., and Sander, R.: A mechanism for halogen release from sea-salt aerosol in the remote marine
989 boundary layer, *Nature*, 383, 327–330, 1996
990
- 991 Vogt, R., Sander, R., von Glasow, R., and Crutzen, P. J.: Iodine chemistry and its role in halogen activation and
992 ozone loss in the marine boundary layer: A model study, *J. Atmos. Chem.*, 32, 375–395, 1999
993
- 994 Volkamer, R., Baidar, S., Campos, T.L., Coburn, S., DiGangi, J.P., Dix, B., Eloranta, E.W., Koenig, T.K., Morley,
995 B., Ortega, I., Pierce, B.R., Reeves, M., Sinreich, R., Wang, S., Zondlo, M.A., and Romashkin, P.A.: Aircraft
996 measurements of BrO, IO, glyoxal, NO₂, H₂O, O₂-O₂ and aerosol extinction profiles in the tropics: comparison
997 with aircraft-/ship-based in situ and lidar measurements, *Atmos. Meas. Tech.*, 8, 2121–2148, doi:10.5194/amt-8-
998 2121-2015, 2015
999
- 000 von Glasow, R., von Kuhlmann, R., Lawrence, M. G., Platt, U., Crutzen, P. J.: Impact of reactive bromine
001 chemistry in the troposphere, *Atmos. Chem. Phys.*, 4, 2481–2497, 2004
002
- 003 Wang, Y., Jacob, D.J., and Logan, J.A.: Global simulation of tropospheric O₃-NO_x-hydrocarbon chemistry 1.
004 Model formulation, *J. Geophys. Res.*, 103, 10713–10725, doi:10.1029/98jd00158, 1998
005
- 006 Wang, Q., Jacob, D.J., Fisher, J.A., Mao, J., Leibensperger, E.M., Carouge, C.C., Le Sager, P., Kondo, Y.,
007 Jimenez, J.L., Cubison, M.J., and Doherty, S.J.: Sources of carbonaceous aerosols and deposited black carbon in
008 the Arctic in winter-spring: implications for radiative forcing, *Atmos. Chem. Phys.*, 11, 23, 12453-12473,
009 doi:10.5194/acp-11-12453-2011, 2011
010



- 011 Wang, S.-Y., Schmidtd, J., Baidar, S., Coburn, S., Dix, B., Koenig, T., Apel, E., Bowdalo, D., Campos, T.,
012 Eloranta, E., Evans, M., DiGangii, J., Zondlo, M., Gao, R.-S., Haggerty, J., Hall, S., Hornbrook, R., Jacob, D.,
013 Morley, B., Pierce, B., Reeves, M., Romashkin, P., ter Schure, A., and Volkamer, R.: Active and widespread
014 halogen chemistry in the tropical and subtropical free troposphere, *P. Natl. Acad. Sci. USA*, 112, 9281–9286,
015 doi:10.1073/pnas.1505142112, 2015
016
- 017 Wesely, M.L.: Parameterization of surface resistance to gaseous dry deposition in regional-scale numerical
018 models, *Atmos. Environ.*, 23, 1293–1304, 1989
019
- 020 Whalley, L. K., Furneaux, K. L., Gravestock, T., Atkinson, H. M., Bale, C. S. E., Ingham, T., Bloss, W. J., Heard,
021 D. E.: Detection of iodine monoxide radicals in the marine boundary layer using laser induced fluorescence
022 spectroscopy, *J. Atmos. Chem.*, 58(1), 19–39, 2007
023
- 024 Whalley, L.K., Furneaux, K.L., Goddard, A., Lee, J.D., Mahajan, A., Oetjen, H., Read, K.A., Kaaden, N.,
025 Carpenter, L.J., Lewis, A.C., Plane, J.M.C., Saltzman, E.S., Wiedensohler, A., Heard, D.E.: The chemistry of OH
026 and HO₂ radicals in the boundary layer over the tropical Atlantic Ocean, *Atmos. Chem. Phys.*, 10, 1555-1576,
027 2010
028
- 029 Whalley, L.K., Blitz, M.A., Desservettaz, M., Seakins, P.W., and Heard, D.E.: Reporting the sensitivity of laser-
030 induced fluorescence instruments used for HO₂ detection to an interference from RO₂ radicals and introducing a
031 novel approach that enables HO₂ and certain RO₂ types to be selectively measured, *Atmos. Meas. Tech.*, 6, 3425-
032 3440, 2013, doi:10.5194/amt-6-3425-2013
033
- 034 Wild, O., Zhu, X., and Prather, M.J.: Fast-J: Accurate Simulation of In- and Below-Cloud Photolysis in
035 Tropospheric Chemical Models, *J. Atmos. Chem.*, 37, 245–282, doi:10.1023/a:1006415919030, 2000
036
- 037 Yan, C., Kocevskaa, S., and Krasnoperov, L.N.: Kinetics of the reaction of CH₃O₂ radicals with OH studied over
038 the 292-526 K temperature range, *J. Phys. Chem. A*, 120, 6111-6121, 2016
039
- 040 Yang, X., Cox, R. A., Warwick, N. J., Pyle, J. A., Carver, G. D., O'Connor, F. M., Savage, N. H.: Tropospheric
041 bromine chemistry and its impacts on ozone: A model study, *J. Geophys. Res.*, 110, D23311,
042 doi:10.1029/2005JD006244, 2005
043
- 044 Zhang, L., Jacob, D.J., Liu, X., Logan, J.A., Chance, K., Eldering, A., and Bojkov, B.R.: Intercomparison methods
045 for satellite measurements of atmospheric composition: application to tropospheric ozone from TES and OMI,
046 *Atmos. Chem. Phys.*, 10, 4725–4739, doi:10.5194/acp-10-4725-2010, 2010
047



048 **Figures**

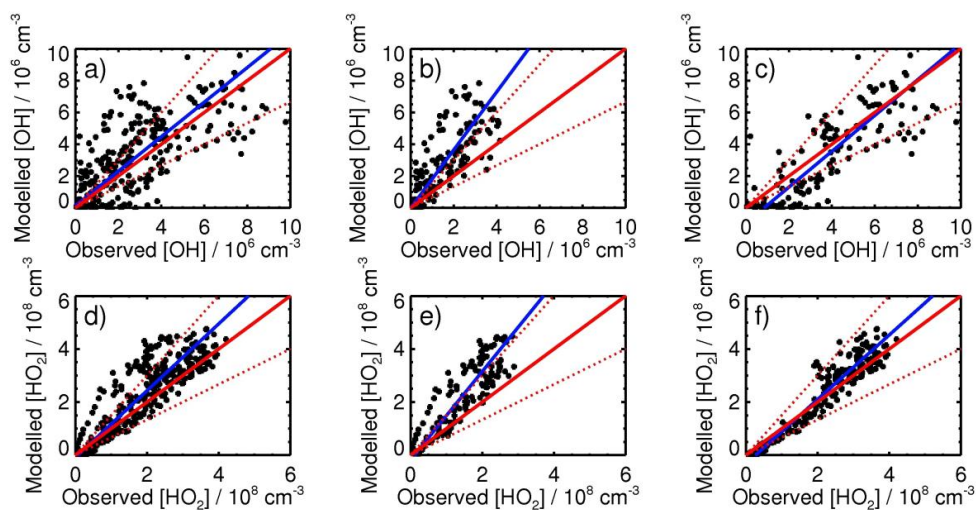


049

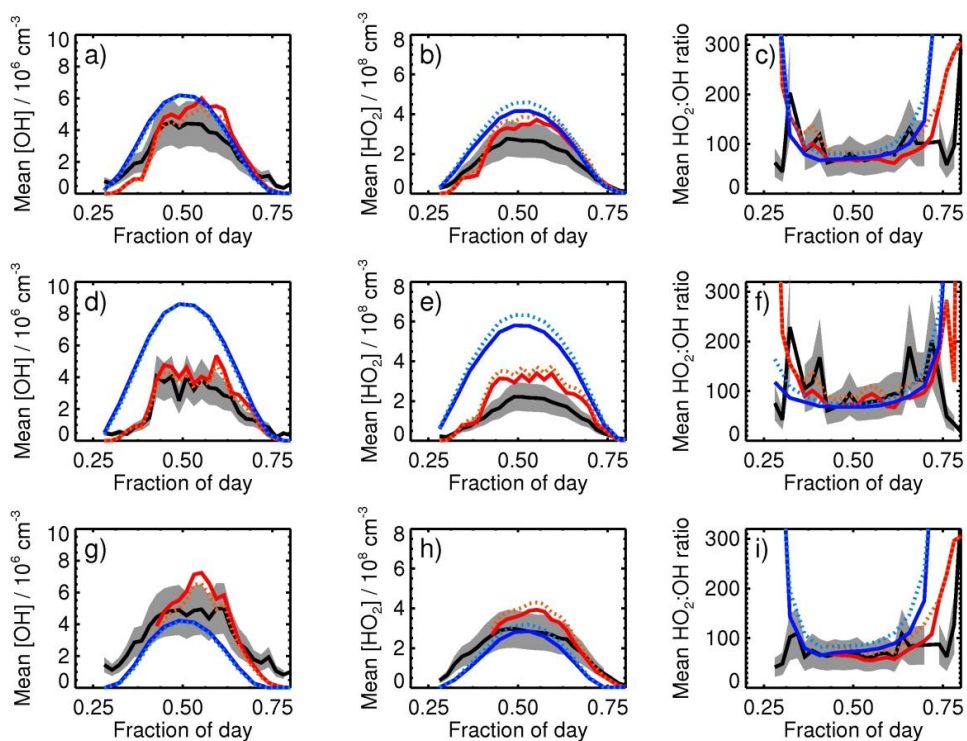
050

051 Figure 1: Observed and modelled concentrations of a) OH during SOS1 (February-March 2009, days 58-68); b)
052 OH during SOS2 (May-June 2009, days 157-168); c) HO_2 during SOS1; d) HO_2 during SOS2. Observed data are
053 shown in black; box model concentrations with halogen chemistry are shown by filled red circles; box model
054 concentrations without halogen chemistry are shown by open orange triangles; global model concentrations with
055 halogen chemistry are shown by solid dark blue lines; global model concentrations without halogen chemistry
056 are shown by broken blue lines.

057



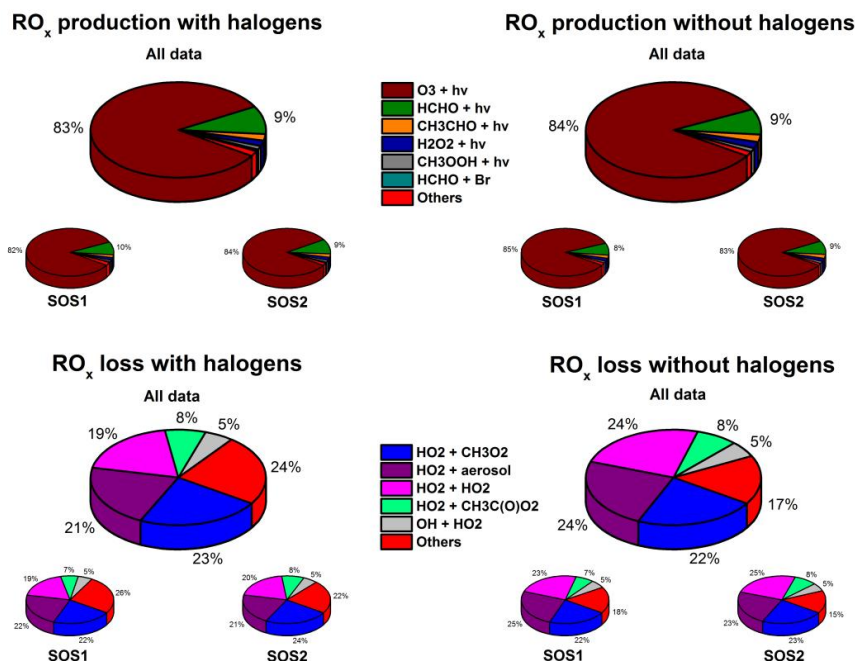
058
 059 Figure 2: Comparison of modelled and observed concentrations of a) OH during SOS1 (February-March 2009)
 060 and SOS2 (May-June 2009); b) OH during SOS1; c) OH during SOS2; d) HO₂ during SOS1 and SOS2; e) HO₂
 061 during SOS1; f) HO₂ during SOS2. In each plot, the solid red line indicates the 1:1 line, with 50 % limits given
 062 by the broken red lines. The best fit lines are shown in blue and are described by a) $[\text{OH}]_{\text{mod}} = (1.09 \pm 0.11) \times$
 063 $[\text{OH}]_{\text{obs}} + (0.13 \pm 0.38) \times 10^6$ ($r^2 = 0.49$); b) $[\text{OH}]_{\text{mod}} = (1.82 \pm 0.26) \times [\text{OH}]_{\text{obs}} - (0.01 \pm 0.51) \times 10^6$ ($r^2 = 0.56$);
 064 c) $[\text{OH}]_{\text{mod}} = (1.11 \pm 0.15) \times [\text{OH}]_{\text{obs}} - (0.95 \pm 0.66) \times 10^6$ ($r^2 = 0.64$); d) $[\text{HO}_2]_{\text{mod}} = (1.26 \pm 0.10) \times$
 065 $[\text{HO}_2]_{\text{obs}} - (0.08 \pm 0.22) \times 10^8$ ($r^2 = 0.77$); e) $[\text{HO}_2]_{\text{mod}} = (1.66 \pm 0.21) \times [\text{HO}_2]_{\text{obs}} - (0.17 \pm 0.34) \times 10^8$ ($r^2 = 0.78$); f) $[\text{HO}_2]_{\text{mod}}$
 066 $= (1.21 \pm 0.12) \times [\text{HO}_2]_{\text{obs}} - (0.32 \pm 0.30) \times 10^8$ ($r^2 = 0.91$).
 067



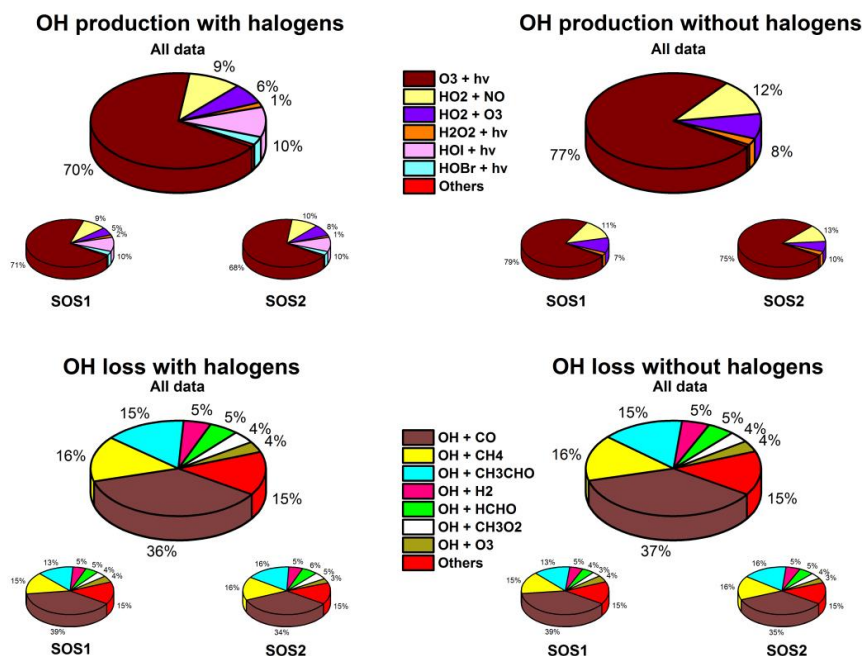
068

069 Figure 3: Average diurnal profiles during the Seasonal Oxidant Study (SOS) at the Cape Verde Atmospheric
070 Observatory for a) OH during both measurement periods; b) HO₂ during both measurement periods; c) HO₂:OH
071 ratio during both measurement periods; d) OH during SOS1 (Feb-Mar 2009); e) HO₂ during SOS1; f) HO₂:OH
072 during SOS1; g) OH during SOS2 (May-June); h) HO₂ during SOS2; i) HO₂:OH ratio during SOS2. Observed
073 data are shown in black, with grey shading indicating the variability in the observations; box model output with
074 halogen chemistry is shown by solid red lines; box model output without halogen chemistry is shown by broken
075 orange lines; global model output with halogen chemistry is shown by solid dark blue lines; global model output
076 without halogen chemistry is shown by broken blue lines.

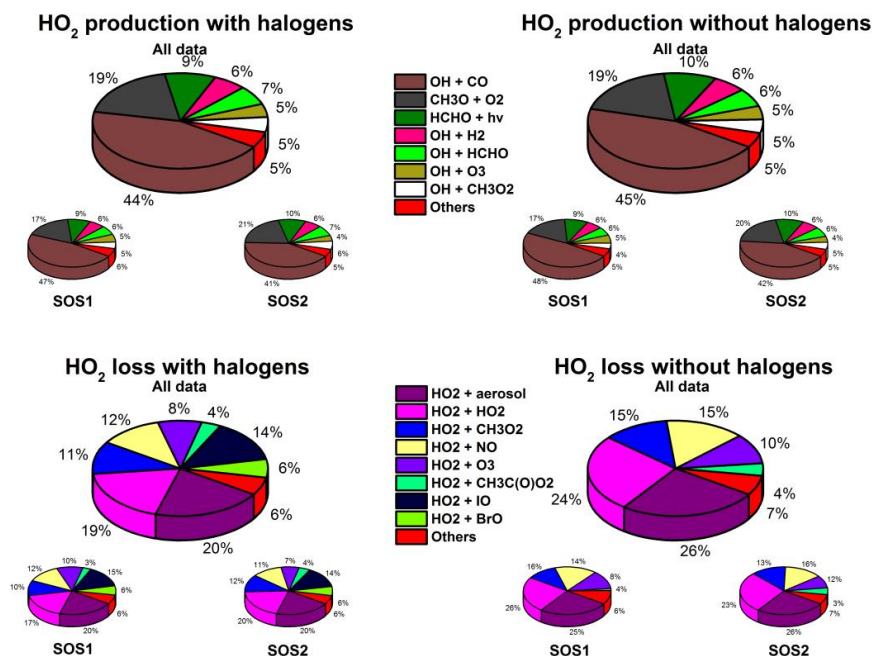
077



078
079 Figure 4: Processes controlling the a) instantaneous RO_x radical production (with RO_x defined here as
080 OH+HO₂+HOBr+HOI+RO+RO₂ owing to the rapid processing between HO₂ and HOBr/HOI) around noon
081 (1100-1300 hours) for box model simulations with halogen chemistry; b) the instantaneous RO_x radical
082 production around noon for box model simulations without halogen chemistry; c) the instantaneous RO_x radical
083 loss around noon for box model simulations with halogen chemistry; d) the instantaneous RO_x radical loss around
084 noon for box model simulations without halogen chemistry. The main charts show the average results for
085 SOS1+SOS2, with results for SOS1 and SOS2 shown separately in the inset charts.



086
087 Figure 5: Processes controlling the a) instantaneous OH radical production around noon (1100-1300 hours) for
088 box model simulations with halogen chemistry; b) the instantaneous OH radical production around noon for box
089 model simulations without halogen chemistry; c) the instantaneous OH radical loss around noon for box model
090 simulations with halogen chemistry; d) the instantaneous OH radical loss around noon for box model simulations
091 without halogen chemistry. The main charts show the average results for SOS1+SOS2, with results for SOS1
092 and SOS2 shown separately in the inset charts.

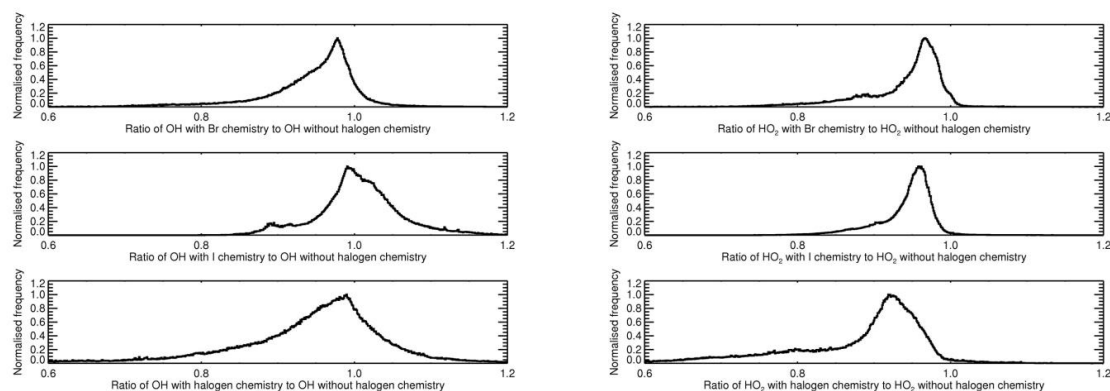


093
 094 Figure 6: Processes controlling the a) instantaneous HO₂ radical production around noon (1100-1300 hours) for
 095 box model simulations with halogen chemistry; b) the instantaneous HO₂ radical production around noon for box
 096 model simulations without halogen chemistry; c) the instantaneous HO₂ radical loss around noon for box model
 097 simulations with halogen chemistry; d) the instantaneous HO₂ radical loss around noon for box model simulations
 098 without halogen chemistry. The main charts show the average results for SOS1+SOS2, with results for SOS1
 099 and SOS2 shown separately in the inset charts.
 100



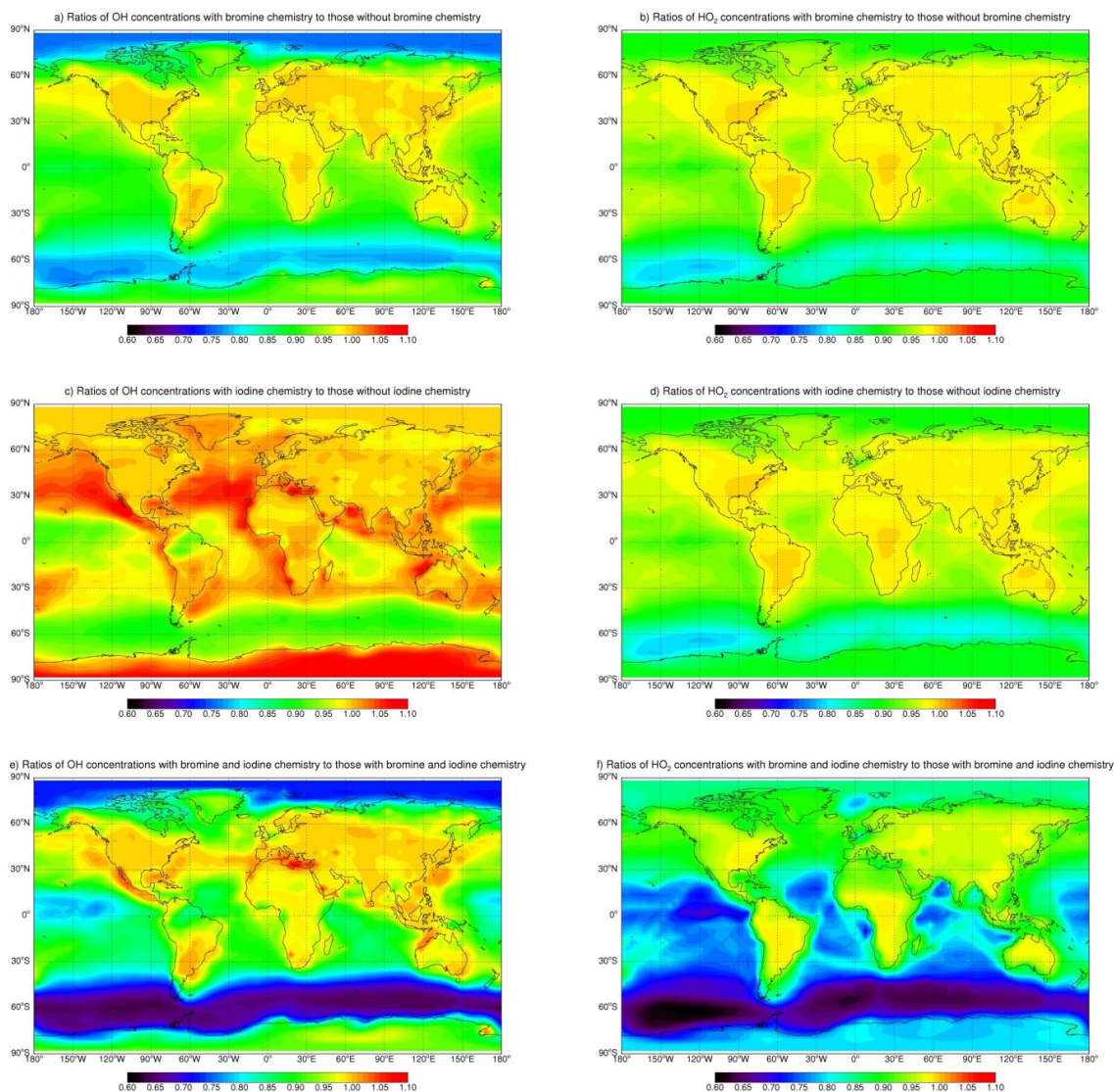
101

102

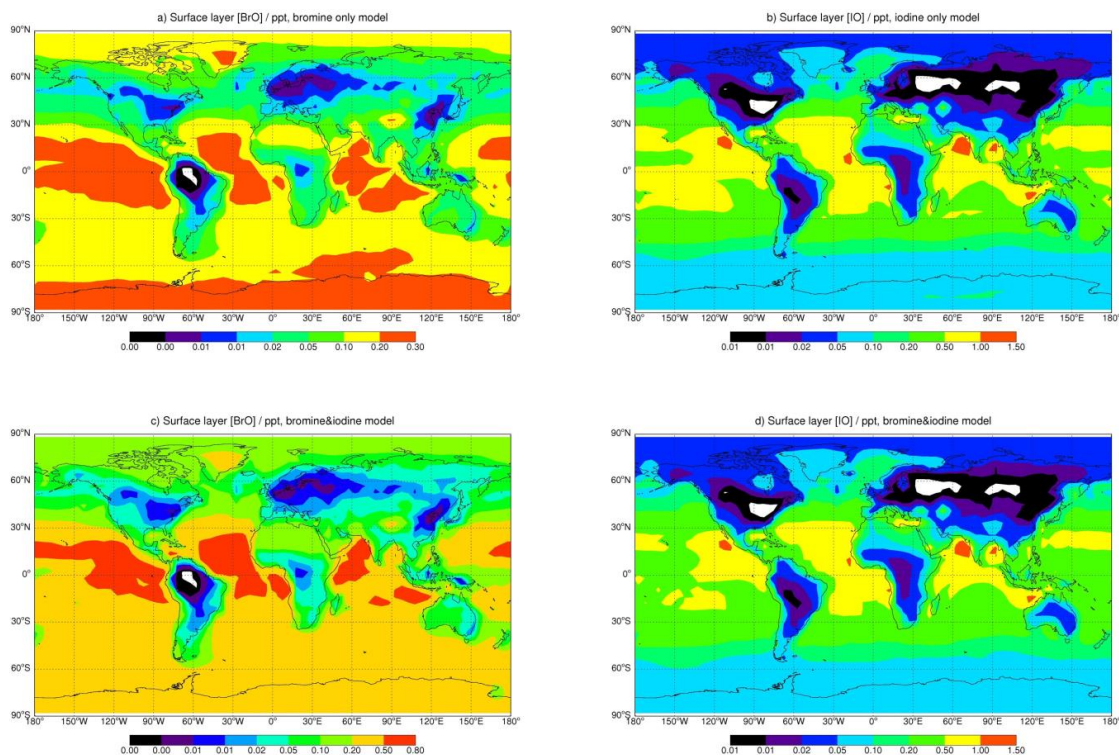


103

104 Figure 7: Normalised probability distribution functions showing the fractional changes in OH (left hand side) and
105 HO₂ (right hand side) in GEOS-Chem for all grid boxes on inclusion of bromine chemistry (upper panels), iodine
106 chemistry (middle panels) and bromine and iodine chemistry combined (lower panels).



107
108 Figure 8: Percentage changes to annual surface layer concentrations of OH (left hand side) and HO₂ (right hand
109 side) in GEOS-Chem on inclusion of bromine chemistry (upper panels), iodine chemistry (middle panels) and
110 bromine and iodine chemistry combined (lower panels).



111
112 Figure 9: Annual surface layer mixing ratios (ppt) of BrO and IO radicals in GEOS-Chem for model runs with
113 just bromine chemistry (upper left panel), just iodine chemistry (upper right panel) and bromine and iodine
114 chemistry combined (lower panels).

115
116
117